Materials Today Bio 31 (2025) 101578

Contents lists available at ScienceDirect

Materials Today Bio

journal homepage: www.journals.elsevier.com/materials-today-bio

Near-infrared light-responsive nanocomposite hydrogels loaded with epidermal growth factor for diabetic wound healing

Li Miao [a,1], Xue Lu [a,1], Yaoyao Wei [a], Jie Zhou [a], Yuanyuan Liu [a], Yang Zhang [a], Changle Meng [c], Mingyang Li [a], Hua Zhang [a,b,*], Wen Chen [a,**], Han Zhang [c,***]

[a] Key Laboratory of Xinjiang Phytomedicine Resource and Utilization of Ministry of Education, School of Pharmacy, Shihezi University, Shihezi, 832003, China
[b] Key Laboratory of Environmental Monitoring and Pollutant Control of Xinjiang Bingtuan, School of Chemistry and Chemical Engineering, Shihezi University, Xinjiang, 832003, China
[c] College of Physics and Optoelectronic Engineering, Shenzhen University, Shenzhen, 518060, China

ARTICLE INFO

Keywords:
Diabetic chronic wounds
MXene
Polymer
Epidermal growth factor
Hydrogel
Wound healing

ABSTRACT

In diabetic wounds, the presence of hyperglycemia is often accompanied by a persistent inflammatory response, oxidative stress damage, impaired angiogenesis and bacterial infections around the wound, resulting in impaired proliferation of dermal and epidermal cells and impaired skin regeneration in diabetic wounds. To solve the above problems, this study designed a near-infrared (NIR) light-responsive multifunctional poloxamer hydrogel (EGF/PDA-MXene Gel). The Gel is composed of two-dimensional nanomaterials (2D NMs) MXene as the core, modified by polymer, further loaded with epidermal growth factor (EGF), and has antibacterial, antioxidant, photothermal properties. Meanwhile, EGF/PDA-MXene Gel can be used as a drug repository, alleviating the problem of short half-life, and realizing the sustained release of EGF. The NIR photothermal property induces protein denaturation leading to the death of pathogenic bacteria, avoiding the common clinical problem of antibiotic resistance. In addition, EGF/PDA-MXene Gel promotes diabetic chronic wound healing by promoting epidermal regeneration, collagen deposition, angiogenesis, and several other mechanisms. Therefore, the Gel preparation strategies that combine bioactive molecules with 2D NMs, which maintains the activity of EGF while exploiting the antimicrobial advantages of 2D NMs photothermally, provide a new and promising therapeutic approach for accelerating the repair of chronic infected wounds.

1. Introduction

In recent years, chronic wounds have emerged as a challenging clinical issue. With the increase in predisposing factors such as aging, diabetes, and obesity, the incidence of chronic wounds has grown exponentially, leading to frequent hospitalizations, infections, and even deaths among patients, which significantly impacts their quality of life [1]. Diabetic foot ulcers (DFUs) are the most typical chronic wounds that fail to heal or have delayed healing due to impaired metabolism, low immunity, and recurrent infections [2–6]. Currently, diabetic wound healing is mainly improved by antibiotics to inhibit bacterial proliferation [7], surgical debridement [8], negative pressure therapy [9], skin substitute grafting [10], and other treatment methods. However, there are drawbacks such as antibiotic resistance, secondary injury due to ordinary wound dressing replacement, high medical cost of skin substitute grafts and reduced efficacy due to frequent administration of single drugs, which seriously limit its clinical application [11]. Therefore, it is necessary to propose a comprehensive diabetic wound healing treatment strategy with antioxidant, antibacterial, epidermal regeneration and angiogenesis effects.

* Corresponding author. Key Laboratory of Xinjiang Phytomedicine Resource and Utilization of Ministry of Education, School of Pharmacy,Shihezi University, Shihezi, 832003, China.
** Corresponding author.
*** Corresponding author.
E-mail addresses: 20212115035@stu.shzu.edu.cn (L. Miao), 20222115005@stu.shzu.edu.cn (X. Lu), weiyaoyao@stu.shzu.edu.cn (Y. Wei), 1209922171@qq.com (J. Zhou), 1960455748@qq.com (Y. Liu), 3121253819@qq.com (Y. Zhang), mengchangle2021@163.com (C. Meng), 1376674842@qq.com (M. Li), zh_pha@shzu.edu.cn (H. Zhang), chen-wen2000@126.com (W. Chen), hzhang@szu.edu.cn (H. Zhang).
[1] Li Miao, Xue Lu contributed equally to this work.

https://doi.org/10.1016/j.mtbio.2025.101578
Received 5 December 2024; Received in revised form 5 February 2025; Accepted 14 February 2025
Available online 14 February 2025

EGF, as a growth factor with extensive physiological activities [12–14], plays an indispensable role in the remodeling phase of wound tissue [15]. Clinically, EGF is often used in combination with antibiotics or corticosteroidal drugs to control infection while promoting wound healing, thereby enhancing therapeutic efficacy. It is noteworthy that locally applied soluble EGF can be degraded by proteases and is readily removed by wound exudates before reaching the deeper layers of the wound. This necessitates frequent administrations to maintain sufficient EGF levels in the wound area, which increases treatment costs. Additionally, excessive EGF diffusion may have adverse effects on surrounding healthy tissues. However, overly frequent administrations may alter the skin's tissue growth environment, leading to secondary bacterial infections and scarring. Therefore, there is an urgent need to develop a wound dressing that can eliminate bacteria, alleviate excessive inflammation, and promote wound healing simultaneously, in order to avoid the issue of antibiotic resistance that arises from the combined use of EGF and antibiotics.

Two-dimensional nanomaterials (2D NMs) with ultra-thin thickness, flexible and controllable dimensions, unique photothermal properties, and favorable biocompatibility are promising for biomedical applications [16]. MXene, as a novel two-dimensional layered nanomaterial composed of transition metal carbides, nitrides, and carbon-nitrides, has often been used as a drug carrier in recent years in drug delivery, regenerative medicine, and other fields due to its large specific surface area [17,18] and high photothermal conversion efficiency [19,20]. For example, a multifunctional MXene-doped photothermal microneedle with excellent mechanical strength, photothermal antimicrobial and reactive oxygen species (ROS) scavenging capabilities was developed for drug-resistant infected wound healing [21]. Polydopamine (PDA) exhibits strong adhesion [22,23], good biocompatibility [24,25], excellent photothermal conversion [26–28], outstanding free radical scavenging activity [29], and its abundance of functional groups (quinone groups, phenolic hydroxyls, and amines) allows it to be often used as an intermediate linker [30–33] to immobilize biologically active molecules and pharmaceuticals onto the surfaces of various materials. In addition, adding PDA to the nanosystem can improve its antibacterial and anti-inflammatory capabilities [34].

Compared to other forms of dressings such as gauze and bandages, hydrogel-based dressings provide a solution for protein storage and controlled delivery by keeping the wound moist, adequately absorbing tissue exudate, being easy to load and delaying drug release, and their dense mesh structure protects the encapsulated drug by restricting the penetration of external enzymes [35]. Its ability to adapt to the shape and size of the wound and minimize the chance of secondary injury due to dressing changes makes it particularly suitable for use in the treatment of diabetic-type chronic wound healing, and it has a greater prospect of clinical translation in infected wounds [36,37].

In this study, a multifunctional hydrogel slow-release drug delivery system was developed (Fig. 1). PDA was selected to modify monolayer MXene nanosheets followed by loading of EGF, and the prepared nanosheets were characterized by a series of characterization tools in terms of their microscopic morphology, elemental composition, and physical phase composition. The nanosheets were embedded in Poloxamer 407 (P407) and Poloxamer 188 (P188) to prepare EGF/PDA-MXene temperature-sensitive hydrogels (EGF/PDA-MXene Gel), and their rheological properties, skin adhesion, antioxidant properties, and photothermal properties were investigated. In addition, the hydrogels were evaluated for their in vitro photothermal antimicrobial, cytocompatibility, and cell migration capabilities. Finally, the hydrogel's ability to promote chronic wound healing was evaluated by a diabetic chronic wound healing assay. The results showed that MXene-based multifunctional hydrogels loaded with EGF could accelerate the

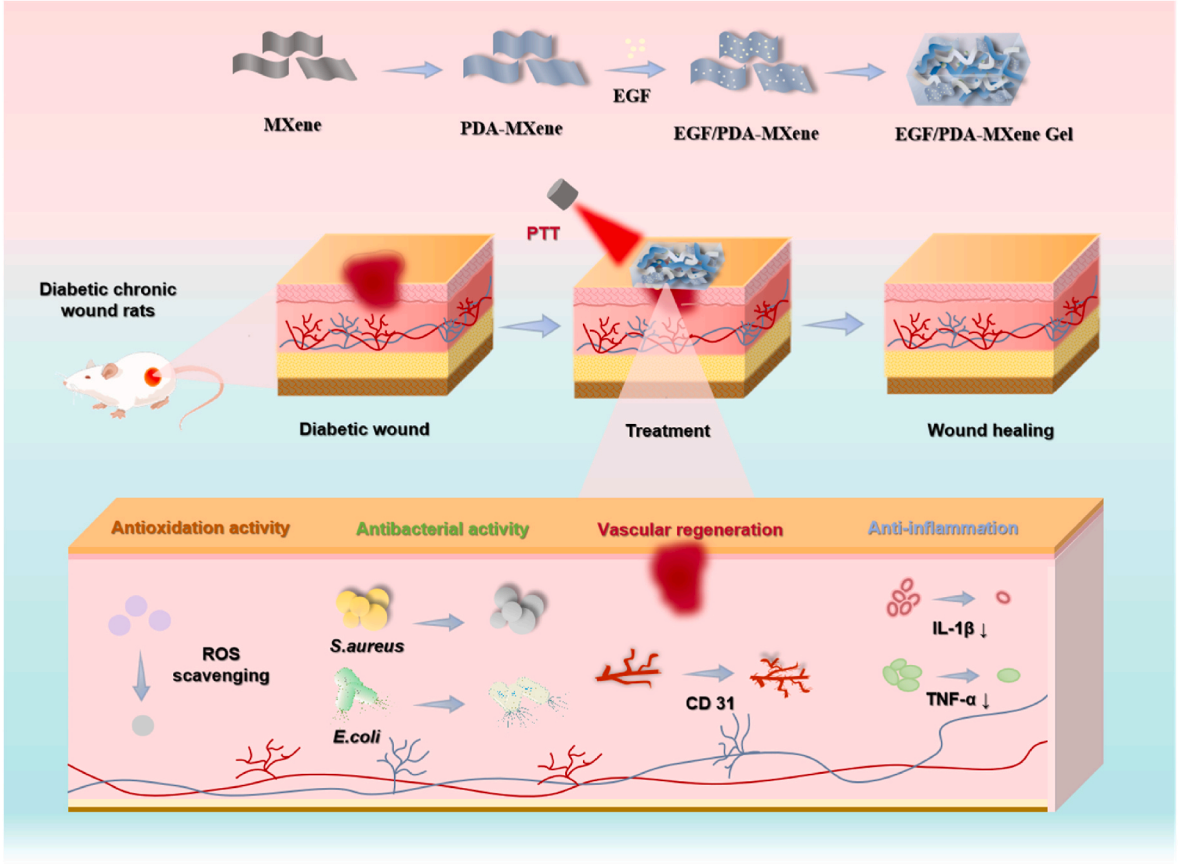

Fig. 1. Preparation and application of a multifunctional EGF/PDA-MXene Gel for chronic wound healing in diabetes.

wound healing process at different stages of wound healing, which provided new ideas for solving the clinical problems associated with chronic wounds.

2. Materials and methods

2.1. Materials

Titanium aluminum carbide was obtained from Beijing Fusman Technology Co., Ltd, LiF, and dopamine hydrochloride were purchased in Shanghai Aladdin Biochemical Technology Co., Ltd. Epidermal growth factor (EGF), LB agar, and nutrient agar were acquired from Shanghai Maclin Biochemical Technology Co., Ltd. Trimethylol aminomethane (Tris) and streptozotocin (STZ) were obtained from Beijing Solaibao Technology Co., Ltd. Poloxamer 407 (P407) and Poloxamer 188 (P188) were supplied by Beijing Ita Biotechnology Co., Ltd. Minimum Essential Medium (MEM), fetal bovine serum (FBS), penicillin-streptomycin Solution, and trypsin-EDTA were procured from Procell Life Science&Technology Ltd. Cell Counting Kit-8 (CCK-8) and Calcein/PI Live/Dead Cytotoxicity Assay Kit were bought from Beyotime Biotechnology. L929 cells were supplied by the Cell Bank of Typical Culture Collection of the Chinese Academy of Sciences, Staphylococcus aureus (*S.aureus*, BNCC310011) and Escherichia coli *(E.coli*, BNCC336435) were purchased from Institute of Microbiology, Chinese Academy of Sciences. Sprague-Dawley rats (SD rats) were obtained from the Medical Laboratory Animal Center, Xinjiang Medical University.

2.2. Preparation of MXene nanosheets

Weigh and dissolve 1.0 g of LiF in 5 mL of deionized water, followed by the slow addition of 15 mL of HCl (9 M) while stirring until complete dissolution. Subsequently, slowly add 1.0 g of Ti_3AlC_2 over 15 min. The entire reaction system should be stirred at 35 °C for 24 h at 500 rpm. After completion, centrifuge the mixture at 5000 rpm at 4 °C for 5 min, then proceed with resuspension precipitation and centrifugation using a solution containing HCl at a concentration of 1 mol/L. The resulting centrifugal products should be alternatively rinsed with deionized water and anhydrous ethanol until pH levels between 5.0 and 6.0. Following this, subject the precipitated reaction product to ultrasonic stripping using deionized water dispersed in an ice water bath under nitrogen protection for 2 h. Subsequently, collect the supernatant was through centrifugation at 3500 rpm for 1 h at 4 °C while ensuring nitrogen protection was maintained throughout this process to obtain a single-layer MXene nanosheets solution, which was stored at 4 °C.

2.3. Preparation of PDA-MXene nanosheets

Measure 20 mL 2.5 mg/mL MXene nanosheets solution, add 100 mg dopamine hydrochloride, stirring for 1 h. Add 100 mL 50 mM Tris-HCl (tris(hydroxymethyl)aminomethane) (pH = 8.5). The whole reaction system was stirred at 25 °C for 8 h at 400 rpm. End of the reaction, the solution was spun off at 4000 rpm for 10 min at 4 °C and then washed three times alternately with deionized water and anhydrous alcohol to eliminate unreacted dopamine. The reaction precipitate was dispersed with deionized water and transferred to brown marshmallow flasks. PDA-MXene nanosheets solution was collected and stored at 4 °C.

2.4. Preparation of EGF/PDA-MXene nanosheets

100 μg of EGF was dispersed in 1 mL of deionized water, and the volume of PBS was constant to 10 mL to obtain EGF stock solution, which contained 1×10^6 units of EGF. 1 mL of EGF stock solution was added into 10 mL 1 mg/mL PDA-MXene nanosheets solution, and the whole reaction system was incubated at 37 °C at 100 rpm for 12 h. Following the reaction, the composite was centrifuged at 4000 rpm for 10 min, and the precipitate was dried in a vacuum oven at 40 °C. The EGF/PDA-MXene nanosheets were collected and stored at 4 °C.

2.5. Preparation of hydrogels

P407 26.033 % and P188 6.059 % were obtained by taking P407 7.0899 g and P188 1.8177 g, grinding them thoroughly, and dissolving them in 30 mL of deionized water respectively. Accurately weigh 1 mg each of MXene, PDA-MXene, and EGF/PDA-MXene powder, add 26.033 % P407 3.016 mL with 6.059 % P188 1 mL, stirring until completely dissolved, and place in the refrigerator at 4 °C to fully dissolve, to obtain MXene Gel, PDA-MXene Gel and EGF/PDA-MXene Gel.

2.6. Characterization

The MXene nanosheets, PDA-MXene nanosheets, and EGF/PDA-MXene nanosheets solutions were ultrasonically dispersed homogeneously, diluted by gradient, and then drop-coated onto carbon-supported film copper mesh (400 mesh). After IR drying treatment, the microscopic morphology was observed using field emission transmission electron microscopy with 200 KV accelerating voltage. The MXene nanosheets solution was ultrasonically dispersed, and drop-coated onto the silicon wafers after gradient dilution, and left to dry to measure the thickness of the samples using an atomic force microscope. The nanosheets powder was mixed and pressed with dried KBr powder and tested to study the changes in chemical bonding in the cross-linking reaction by Fourier Transform Infrared Spectroscopy under vacuum with a test range of 4000-500 cm^{-1} at 4 cm^{-1} resolution. The dynamic light scattering system using laser particle size Zeta potential and absolute molecular weight analyzer was used to examine the nanosheets' particle size distribution and potential changes. The surface structures of the nanomaterials were examined by an X-ray diffractometer to analyze the material composition and crystal structure, with a test range of 2°–80° with a scan rate of 2°/min. The surface elemental compositions, chemical states, and molecular structures of the MXene, PDA-MXene, and EGF/PDA-MXene nanosheets were inspected by X-ray photoelectron spectrometry. The elemental composition of EGF/PDA-MXene nanosheets was visualized by high-resolution field emission transmission electron microscopy. The hydrogel samples were freeze-dried and adhered to conductive adhesive, and the microstructure of the hydrogels was observed by scanning electron microscopy after gold spraying treatment.

2.7. Investigation of rheological properties and adhesion

Blank Gel, MXene Gel, PDA-MXene Gel, and EGF/PDA-MXene Gel were placed in the center of the circular test tray of the rheometer, respectively. The changes of energy storage modulus (G′) and loss modulus (G″) of hydrogels were observed at a constant strain of 1 %, a constant frequency of 1 Hz, and a heating rate of 0.5 °C/min in the temperature interval of 20–60 °C. The oscillation angle frequency was scanned from 100 to 0.1 rad/s at 25 °C and 37 °C, respectively, to examine the relationship between hydrogel viscoelastic properties and frequency.

The hydrogels were placed on the surface of fresh pig skin and mouse skin respectively, and incubated at 37 °C for 10 min in the incubator, and then the gel state of the hydrogels in each group was monitored. The mouse skin was stretched, and the pig skin was placed vertically to observe photographically, and record the morphological changes of the hydrogels.

2.8. Antioxidant properties

MXene Gel, PDA-MXene Gel, and EGF/PDA-MXene Gel were mixed thoroughly with $ABTS^+$ working solution and incubated for 6 min away from light, then the absorbance of the samples was tested at 734 nm, and the color of the solution was recorded. MXene Gel, PDA-MXene Gel, and

EGF/PDA-MXene Gel were mixed thoroughly with $DPPH^+$ working solution and incubated for 30 min away from light. The absorbance of the mixture at 517 nm was measured and the solution color was recorded with a video camera. The free radical scavenging rate was calculated by eq. (1).

$$\text{Scavenging}\ (\%) = \frac{A_0 - (A_S - A_G)}{A_0} \times 100\ \% \quad (1)$$

where: [A_0] represents the absorbance of deionized water + working solution, [A_S] represents the absorbance of hydrogel working solution, [A_G] represents the absorbance of hydrogel + solvent.

2.9. Photothermal properties

Blank Gel, MXene Gel, PDA-MXene Gel, and EGF/PDA-MXene Gel were irradiated with an 808 nm NIR laser emitter for 10 min, and the temperature changes of the samples were recorded at 30 s intervals. The intensity of the laser emitter was adjusted to 0.5, 1.0, 1.5, and 2.0 W/cm^2 to irradiate EGF/PDA-MXene Gel for 10 min, and the temperatures were recorded at 30 s intervals. Different concentrations of EGF/PDA-MXene Gel were irradiated separately for 10 min, and the temperature changes of the samples were recorded every 30 s. Subsequently, after irradiation with 808 nm NIR light for 10 min, the 808 nm NIR light was turned off to allow natural cooling for 10 min, and the above heating cycle was repeated 5 times, and the change of hydrogel temperature was recorded every 30 s. The hydrogel temperature change versus time curve was plotted.

2.10. In vitro drug release

The release of EGF from EGF/PDA-MXene solution, EGF/PDA-MXene Gel, and EGF/PDA-MXene Gel + NIR was investigated separately. 2 mL of 250 μg/mL sample was added to the bottom of a beaker placed in a constant temperature oscillator at 37 °C, 150 mL of PBS (pH = 7.4) was added, with an oscillation rate of 100 rpm. Multiple sampling points were set up at certain time intervals, which were 0.5, 1, 2, 3, 4, 6, 8, 10, 12, 24, 36, and 48 h, and the volume of the sample was 1 mL, and 1 mL was injected after sampling. PBS was injected into the system after sampling to ensure that the total volume of the system remained unchanged. The NIR group was sampled and replenished with PBS at the sampling point and again after irradiation at 808 nm for 10 min. Following the EGF ELISA kit, the absorption was recorded at 450 nm by using an enzyme marker. The cumulative release rate of EGF was calculated according to equation (2), and the release curve of the drug in vitro was plotted:

$$\text{In vitro drug release rate}\ \% = \frac{\text{drug release amount}}{\text{total drug amount}} \times 100\ \% \quad (2)$$

2.11. In vitro stability investigation

To investigate the stability of EGF/PDA-MXene Gel, changes in the appearance properties of EGF/PDA-MXene Gel were observed on days 0, 3, 7, 10, 14, and changes in pH of EGF/PDA-MXene Gel were detected with a pH meter, while EGF was measured to observe changes in content.

2.12. In vitro photothermal antimicrobial assay

S.aureus and *E.coli* were selected, and the strains were added into LB liquid medium and placed in a thermostatic shaking box (37 °C, 180 r/min), and the logarithmic growth period bacterial solution was selected for the experiment. When the concentration of the bacterial solution was 10^8 CFU/mL (OD600 = 0.1), the bacterial solution was mixed with hydrogel at 1:1 and placed in a constant temperature incubator (37 °C, 4 h). After the incubation was completed, 100 μL was taken and added dropwise to the LB agar plate coated evenly and placed in a constant temperature incubator (37 °C, 24 h). Among them, the NIR light group was mixed uniformly and irradiated at 808 nm, 1.5 W/cm^2 power for 5 min, and then placed in the constant temperature incubator for co-incubation to observe the growth of the colonies and take photos to record.

S.aureus and *E.coli* in the logarithmic growth phase were taken respectively, and the concentration of the bacterial solution was adjusted to 1×10^8 CFU/mL after resuspension in 0.9 % saline, and the hydrogel was mixed with the bacterial suspension at 1:1 and incubated at 37 °C for 4 h. After incubation, the hydrogel was centrifuged (6000 rpm, 5 min), washed with physiological saline for two times, and then resuspended to 500 μL, and then stained by DMAO/EthD-III dye under light protection for 15 min. DMAO/EthD-III dye was used for staining, and after incubation for 15 min, 5 μL was taken on a slide and observed and photographed under an orthogonal fluorescence microscope.

2.13. In vitro cell biocompatibility assay

Cell suspensions (100 μL/well) of 5×10^3/well were seeded into 96-well plates and cultured at 37 °C with 5 % CO_2 for 24 h. When the cells had grown to about 80 %, 100 μL of hydrogel complete medium extract with different concentrations was added to each well in the experimental group, and 100 μL of complete medium containing cells (MEM + 10 % FBS + 1 % double antibody) was added to the control group. Repeat six wells per group and continue incubation for 24 or 48 h. After the reaction, 100 μL of medium containing 10 % CCK-8 solution was added to each well, and the absorbance was measured in 450 nm wavelength after incubation for 1 h in a cell culture incubator, and the cell viability was calculated according to eq. (3).

$$\text{Cell survival rate}\ (\%) = \frac{OD_s - OD_k}{OD_d - OD_k} \times 100\ \% \quad (3)$$

where: ODs, ODd, ODk are the OD values at 450 nm for the experimental group, control group and blank group, respectively.

The cells were inoculated with 5×10^4/well cell suspension (1 mL/well) in 12-well plates and incubated in a cell culture incubator at 37 °C with 5 % CO_2 for 24 h. When the cells grew to about 50 %, 500 μL of complete medium was added to the control group, and 500 μL of hydrogel complete medium extract was added to the experimental group to continue to incubate the cells for 24 h or 48 h. After incubation was completed, 500 μL of Calcein AM&PI staining solution was added and incubated for 30 min at 37 °C and protected from light. After the incubation was completed, 500 μL of Calcein AM&PI staining solution was added, and the cells were incubated at 37 °C for 30 min, protected from light, and the fluorescence staining images were observed and recorded.

2.14. Cell scratch assay

The effect of EGF/PDA-MXene Gel on the migration of L929 was evaluated by the cell scratching method. Cell suspensions of 1.5×10^5/well were inoculated in 6-well plates and cultured in a cell culture incubator at 37 °C and 5 % CO_2 for 24 h. After the cells were completely adhered to the wall, they were scratched with a 200 μL tip of a gun, and the floating cells were washed with PBS. Complete medium extracts of Blank Gel, MXene Gel, PDA-MXene Gel, and EGF/PDA-MXene Gel were added respectively to continue the incubation, and the cell migration was observed and recorded at 0 h, 24 h, and 48 h. The cell migration area was counted using Image J, and the cell migration rate was calculated by eq. (4).

$$\text{Cell scratch closure}\ (\%) = \frac{S_0 - S_{\Delta h}}{S_0} \times 100\ \% \quad (4)$$

where: S_{0h} is the area of the scratch on day 0, $S_{\Delta h}$ is the area of the scratch at different time points.

2.15. Experimental chronic wound healing in diabetes mellitus

The animal experimental protocol in this study was approved by the Medical Ethics Committee of the First Hospital Affiliated to the Medical College of Shihezi University (certification number: A2023-278-01) and was performed according to the national regulations on the management of experimental animals. The type I diabetes mellitus model was established by intraperitoneal injection of streptozotocin at the dose of 65 mg/kg in male SD rats at 6–8 weeks of age after one week of acclimatization and feeding. After the blood glucose level exceeded 16.7 mmol/L, anesthesia was administered and hair was removed to expose the dorsal skin and to construct a 1-cm-diameter whole-layer wound model. It was divided into 8 groups (n = 8): Blank group, Control group, Blank Gel group, positive drug group (rhEGF hydrogel), MXene Gel group, PDA-MXene Gel group, EGF/PDA-MXene Gel group, and EGF/PDA-MXene Gel + NIR group (1.5 W/cm^2, 5 min), in which saline was given to the blank group and the model group (the blank group was the wound model of normal SD rats, and the rest of the group was the diabetic SD rats). A sterile syringe was used to instill 0.25 mL of drug or saline to cover the wound surface and the hydrogel was fixed with 3M Tegaderm™. The healing status of the wounds was observed on postoperative days 0, 3, 7, 10, and 14 and recorded with a camera, and the area of each wound was quantitatively analyzed by Image J, and the wound healing rate was calculated by eq. (5).

$$\text{Wound healing rate}\ (\%) = \frac{S_0 - S_N}{S_0} \times 100 \quad (5)$$

where S_0 is the wound area on day 0 and S_N is the wound area at different time points.

2.16. Histological analysis

Wound tissues were collected on days 7 and 14, respectively, fixed in 4 % paraformaldehyde, embedded, and tissue sectioned. H&E staining and Masson staining were used to observe tissue regeneration and collagen deposition. The expression of interleukin-1β (IL-1β) and tumor necrosis factor-α (TNF-α) in the tissue sections was detected by immunohistochemistry. The expression of platelet endothelial cell adhesion molecule-1 (CD31) was determined by immunofluorescence staining. The staining results were analyzed using Image-J software. Blood was collected on day 14 for serum biochemical indexes and organs such as the heart, liver, spleen, lungs, and kidneys were collected and embedded in sections for H&E staining.

2.17. Biocompatibility and safety studies

After the 14-day chronic wound healing experiment was completed, blood was collected from rats for liver and kidney function and routine blood tests. After completion of blood sampling, the rats were euthanized, and major organs such as the heart, liver, spleen, lungs, and kidneys were collected and fixed in paraformaldehyde, embedded in paraffin, and sectioned for H&E staining analysis to assess the in vivo safety of the hydrogel after administration.

2.18. Statistical analysis

GraphPad Prism 8 was used for statistical analysis. Data were expressed as mean ± standard deviation and statistical differences between multiple data sets were assessed by *t*-test or one-way ANOVA. *p < 0.05 was considered as statistically significant difference (*$P < 0.05$, **$P < 0.01$, ***$P < 0.001$, and ****$P < 0.0001$).

3. Results and discussion

3.1. Characterisation of EGF/PDA-MXene gel

In this study, the LiF/HCl etching method was chosen to etch the Al atomic layer from the MAX phase, and the high concentration of acid and Li^+ intercalation showed a multilayered fluffy structure in the interlayer of MXene nanosheets (Fig. 2A), with a size of up to 3 μm. After low-temperature ultrasonic exfoliation, the layer spacing was gradually enlarged, some of the chemical bonding occurred, and the large-size layers were reduced, showing the monolayered MXene nanosheets with smooth edges (Fig. 2B), with transverse sizes in the range of 250–350 nm and thicknesses of about 1.9 nm (Fig. 2C–D), which initially indicated the successful preparation of monolayer MXene nanosheet.

After the modification of MXene nanosheets by polydopamine coating through the self-polymerization of dopamine under weak alkali conditions, a film-like black substance appears on the surface of the PDA-MXene nanosheets compared to the TEM images of the MXene nanosheets, which is presumed to be the result of the self polymerization of PDA on the surface of the MXene nanosheets (Fig. 2E). The results of particle size change before and after PDA modification are shown in Fig. 2F. The particle size of the nanoparticle increases from 281 nm to 352 nm, which may be due to the stacking and adhesion of the nanoparticle due to the adhesion of the PDA itself, and the increase of MXene nanoparticle layer spacing caused by the coating of the PDA. Fig. 2G shows the potential change before and after PDA modification, and the average potential of the nanosheets decreased from −26.67 mV to −31.33 mV after the introduction of PDA.This is due to the fact that PDA is rich in functional groups such as amino and phenolic hydroxyl groups, which have strong electronegativity, and the electronegativity of the composite surface is enhanced when PDA is wrapped on the surface of MXene nanosheets. The increase of electronegativity makes the charge distribution on the surface of MXene nanosheets more uniform, enhances the charge interaction inside the nanosheets, and improves the structural stability of MXene nanosheets. The XRD diffraction spectra patterns of MXene, PDA-MXene, the characteristic peaks of aluminum crystal surface were not observed at 2θ = 39° indicating that Al has been removed by etching and the (002) characteristic peak of MXene was shifted forward from 9.44° to 6.3°, which indicated that the carbon lattice spacing was increased and monolayer MXene nanosheets have been successfully prepared. The PDA-MXene pattern showed no significant change in the diffraction peaks except the (002) characteristic peak was shifted forward to 5.9° (Fig. 2H), which was an increase in the layer spacing due to the PDA coating, in addition, the introduction of PDA did not have any other effect on the crystal structure of MXene.

The load of EGF on the PDA-MXene nanosheets was realized through oscillating culture. Compared with the PDA-MXene nanosheets (Fig. 2E), a large number of tiny black materials were distributed in obvious dots on the EGF/PDA-MXene nanosheets (Fig. 2I), which was preliminarily assumed to be a successful load of EGF. In order to further determine the element composition of the nanosheets, the element distribution of the EGF/PDA-MXene nanosheets was studied by high-resolution field emission transmission electron microscopy, and C, Ti, O, N, and S were detected (Fig. 2J). The presence of S further indicates that EGF has been successfully loaded. To further determine the changes of chemical bonds and functional groups before and after the reaction, FT-IR tests were performed on the nanosheets (Fig. 2K), and the characteristic peaks of the MXene nanosheets appeared at 3404 cm^{-1} and 1645 cm^{-1}, which correspond to the stretching vibrations of -OH and C=O, respectively, whereas the stretching vibration of the C-O bond was observed at 1536 cm^{-1}, and the Ti-O peak appeared at 591 cm^{-1}. The increase in peak intensity at 3404 cm^{-1} of PDA-MXene nanosheets could be attributed to the -OH and -NH_2 of PDA itself and new characteristic peaks appeared at 1625 cm^{-1} and 1475 cm^{-1}, which were attributed to the aromatic ring of PDA and the -OH group of catechols, suggesting that

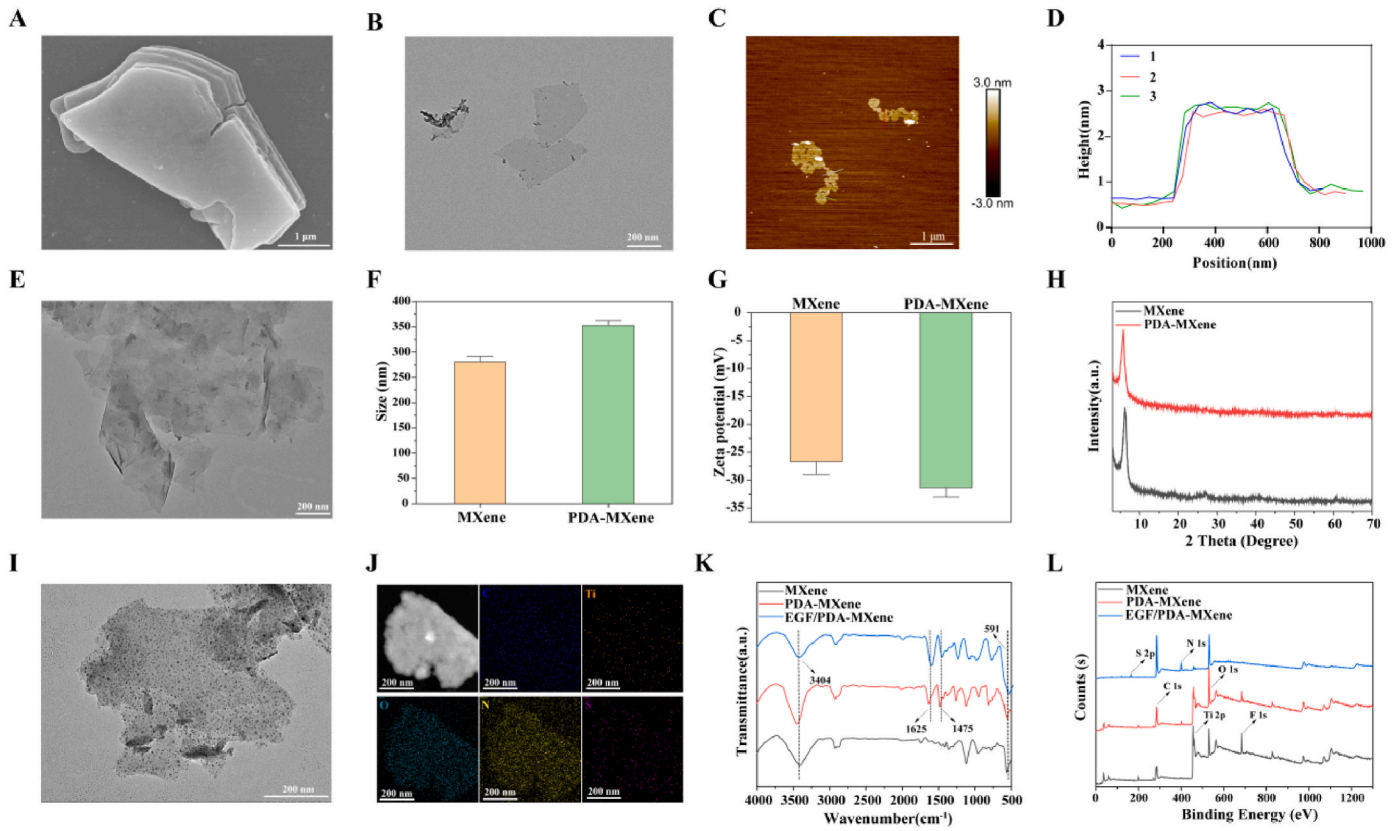

Fig. 2. Nanosheets characterization. (A) SEM images of multilayer MXene nanosheets, (B) TEM images of monolayer MXene nanosheets, (C) AFM images of monolayer MXene nanosheets, (D) Thickness of MXene nanosheets in the AFM maps, (E) TEM images of PDA-MXene nanosheets, (F) Nanosheets particle size maps before and after PDA modification, (G) before and after PDA modification nanosheets potential maps, (H) XRD patterns of MXene and PDA-MXene nanosheets, (I) TEM images of EGF/PDA-MXene nanosheets, (J) Mapping elemental distribution of EGF/PDA-MXene nanosheets, (K) MXene, PDA-MXene and EGF/PDA-MXene nanosheets FT-IR spectra, (L) XPS patterns of MXene, PDA-MXene and EGF/PDA-MXene nanosheets.

the dopamine successfully polymerized on the surface of MXene. The characteristic peaks of the PDA-MXene nanosheets had characteristic peaks from the structural juxtaposition of PDA and MXene nanosheets without significant valence bonding connections and peak shifts, presumably modifying the surface of the material by electrostatic interaction between MXene nanosheets and PDA. The characteristic peaks of EGF/PDA-MXene nanosheets were roughly identical to those of PDA-MXene nanosheets, but the peaks at 3404 cm^{-1} for -OH and -NH_2 peaks at 3404 cm^{-1} were slightly weakened, presumably because EGF, a peptide, was attached to the PDA-MXene nanosheets utilizing hydrogen bonding. The increase in peak intensity at 539 cm^{-1} is attributed to the presence of -S-S- in EGF; the characteristic peak at 1625 cm^{-1} is significantly enhanced compared to the PDA-MXene nanosheets as a result of C=O stretching vibration, which suggests the successful loading of EGF in the PDA-MXene nanosheets, and further corroborates the fact that MXene, PDA-MXene, and EGF/PDA-MXene nanosheets were successfully prepared.

The chemical compositions of MXene, PDA-MXene, and EGF/PDA-MXene nanosheets were analyzed by XPS, and elements such as C, Ti, O and F were detected in the MXene nanosheets, the elements C and Ti were derived from MAX powder, the appearance of O was attributed to the generation of hydroxyl groups of MXene, and the element F was derived from LiF, a result which verified the successful preparation of MXene (Fig. 2L). The appearance of the N 1s peak at 401 eV and the significant decrease in the intensity of the F 1s peak at 685 eV and the Ti 2p peak at 563 eV in the energy spectrum of PDA-MXene indicate the successful introduction of the element N. The appearance of the S 2p peak at 164 eV in the spectrum of EGF/PDA-MXene suggests the presence of the element S, and the intensity of the N 1s peak at 401 eV is greater than that of PDA-MXene, which is due to the presence of disulfide bonds and amino groups in EGF as a small-molecule polypeptide formed from 53 amino acids. The above results confirmed the successful preparation of EGF/PDA-MXene nanosheets.

Considering that the temperature-sensitive hydrogel forms a semi-solid gel under body temperature conditions, the physiological temperature of the human body is 37 °C however, the skin temperature is 33.5 ± 0.5 °C, the gelation temperature should be slightly lower than the skin temperature, therefore, 32 °C was set as the target gelation temperature. The prepared MXene, PDA-MXene, and EGF/PDA-MXene nanosheets were encapsulated in a temperature-sensitive hydrogel, which was able to gel rapidly at 32 °C (Fig. 3A). The microscopic morphology of hydrogels presents a three-dimensional network structure with irregular interconnected pores, which provides for water absorption, drug-carrying, and substance exchange (Fig. 3B).

3.2. Rheological properties

The gelation time was determined by measuring the changes of energy storage modulus (G′) and energy dissipation modulus (G″) in rheological properties. Under the conditions of constant strain of 1 %, constant frequency of 1 Hz, temperature scanning range of 20–60 °C, and heating rate of 0.5 °C/min, the gelling temperatures of Blank Gel, MXene Gel, PDA-MXene Gel, and EGF/PDA-MXene Gel were 32.26 °C, 32.37 °C, 32.44 °C, and 32.46 °C, respectively, which were in line with the expected, with no significant difference (Fig. 3C). As the temperature continued to increase, the hydrophobic group interactions of Poloxamer were stronger, and when G′>G″, the hydrogel showed a semi-solid or immobile solid gel state.

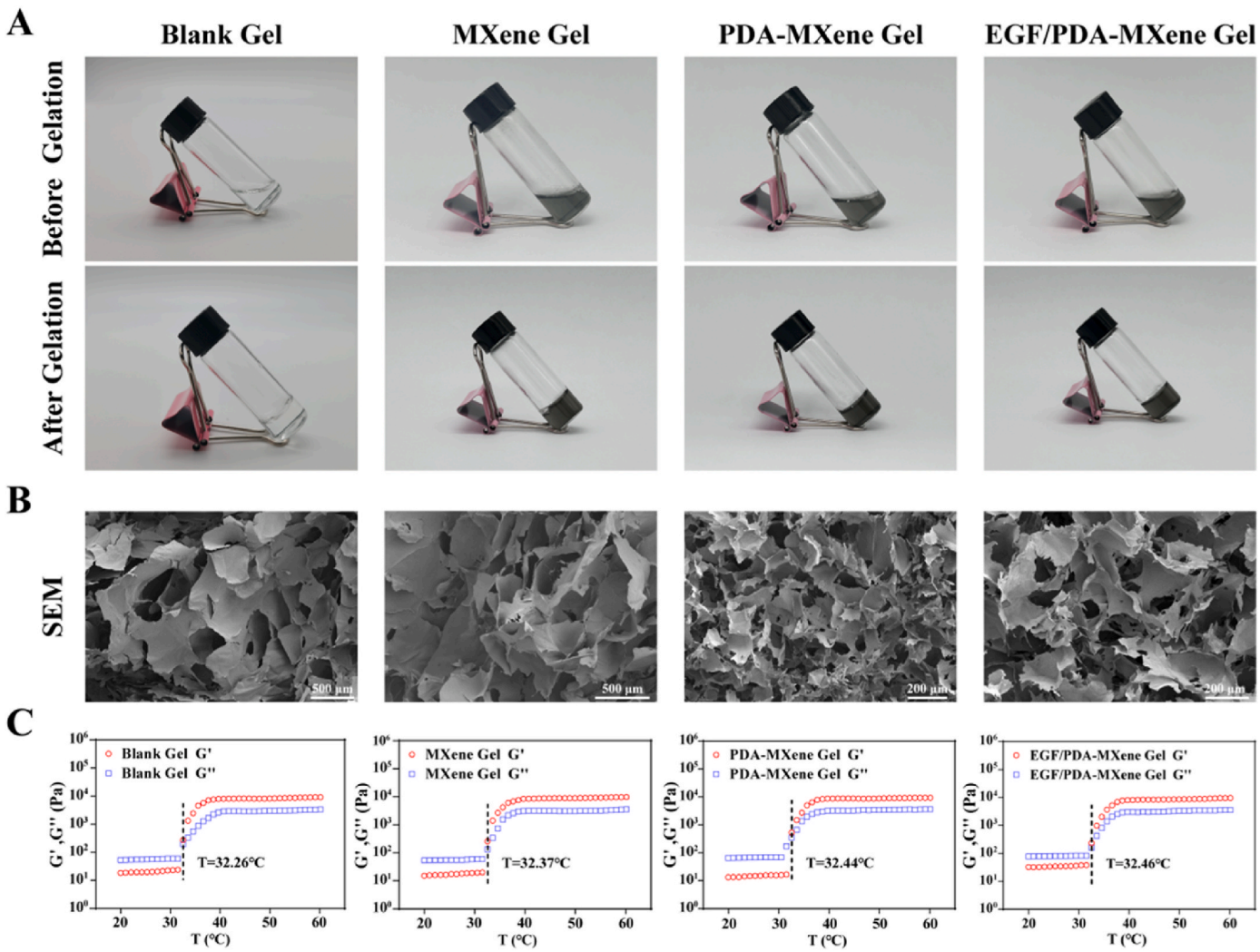

Fig. 3. Characterization of hydrogels. (A) Comparison of the appearance of hydrogels before and after gelling, (B) SEM image of hydrogels after freeze-drying, (C) Dynamic temperature scanning curve of hydrogels.

The changes in viscosity of hydrogels were examined at 25 °C and 37 °C at shear rates of 100 - 0.1 rad/s, respectively. At the same shear rate, the viscosity exhibited EGF/PDA-MXene Gel ≈ PDA-MXene Gel > MXene Gel > Blank Gel, where the higher viscosity of EGF/PDA-MXene Gel and PDA-MXene Gel can be attributed to the introduction of PDA, with a large number of catechol structures conferring superb adhesion (Fig. 4A). In addition, the viscosity of the hydrogel at 37 °C was significantly stronger than that at 25 °C, which was caused by the phase transition of the hydrogel at 32.5 °C and the increase in the resistance to flow. It is worth noting that the viscosity-shear rate curves of the hydrogels all showed a tendency for the viscosity to decrease with increasing shear rate, indicating the ability to shear thinning, suggesting that the hydrogels were all pseudoplastic fluids. When applied to the wound, the friction generated would reduce the viscosity of the hydrogels to enable them to cover the wound more evenly to exert their medicinal effects.

3.3. Adhesion properties

In wound repair, wound dressings with adhesive properties are important for effective wound closure. When the temperature is 25 °C, the hydrogel remains in the sol state when placed horizontally on mouse skin and pig skin. At this time, the hydrogel can flow and cover the skin, but it will not form a stable solid structure, and the adhesion is relatively weak. After being placed at 37 °C, the hydrogel adhered to stretched mouse skin (Fig. 4B) and vertically placed pig skin (Fig. 4C) without detachment or cracking. The above results show that the hydrogel has good skin adhesion and can be well applied to skin wounds.

3.4. Antioxidant properties

In this study, the antioxidant activity of hydrogels was evaluated by detecting the scavenging ability of ABTS free radical and DPPH free radical to simulate the antioxidant ability of hydrogels on various difficult wounds. The hydrogels showed a dosing dependence when the dosing concentration was in the range of 6.25–150 μg/mL, and the scavenging efficiency of ABTS free radicals significantly increased with the increase of dosing concentration (Fig. 4D). 125 μg/mL EGF/PDA-MXene Gel can show considerable free radical scavenging efficiency, while the concentration of MXene Gel and PDA-MXene Gel can reach 90.90 % and 94.91 % of ABTS free radical scavenging efficiency. In addition, the DPPH radical scavenging rate of the hydrogels showed a positive correlation (Fig. 4E). At 150 μg/mL, EGF/PDA-MXene Gel free radical scavenging rate can reach 99.23 %, MXene Gel, PDA-MXene Gel 89.60 % and 96.23 %, which also have high free radical scavenging effect. This is mainly attributed to the quinone structure in the neighboring position of the PDA molecule reacting with HOO· to confer better antioxidant properties to the hydrogels. The color change diagram of

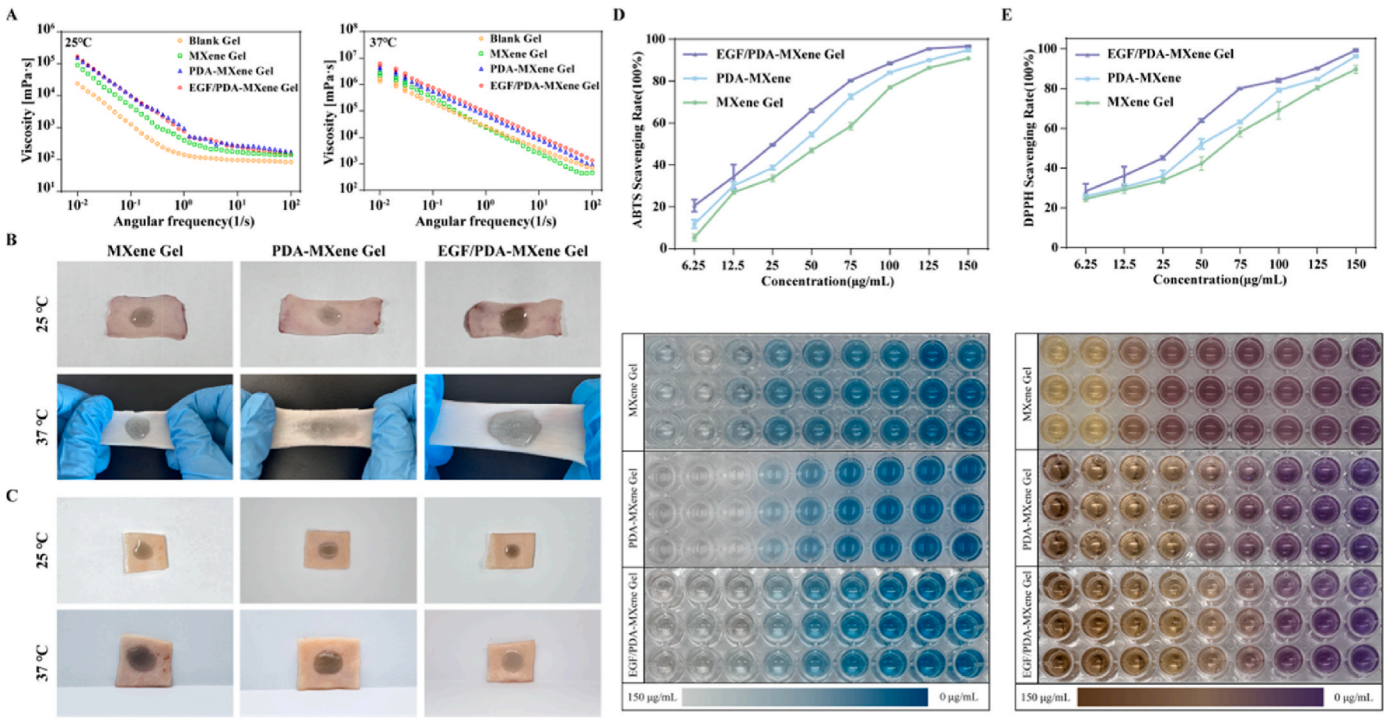

Fig. 4. Adhesion and antioxidant properties of hydrogels. (A) Viscosity changes curves of hydrogels at different temperatures in the interval of shear rate of 0.01–100/s, (B) Adhesion of hydrogels to mouse skin, (C) Adhesion of hydrogels to pig skin, (D) Plot of scavenging rate of free radicals and color change of reaction of ABTS, (E) Plot of DPPH radical scavenging rate and response color change. (For interpretation of the references to color in this figure legend, the reader is referred to the Web version of this article.)

hydrogel working reaction with ABTS and DPPH radical observed that the color of the solution gradually decreased with the increase of drug concentration. These results indicate that MXene Gel, PDA-MXene Gel, and EGF/PDA-MXene Gel can effectively remove ROS, reduce oxidative stress, and exert their antioxidant capacity.

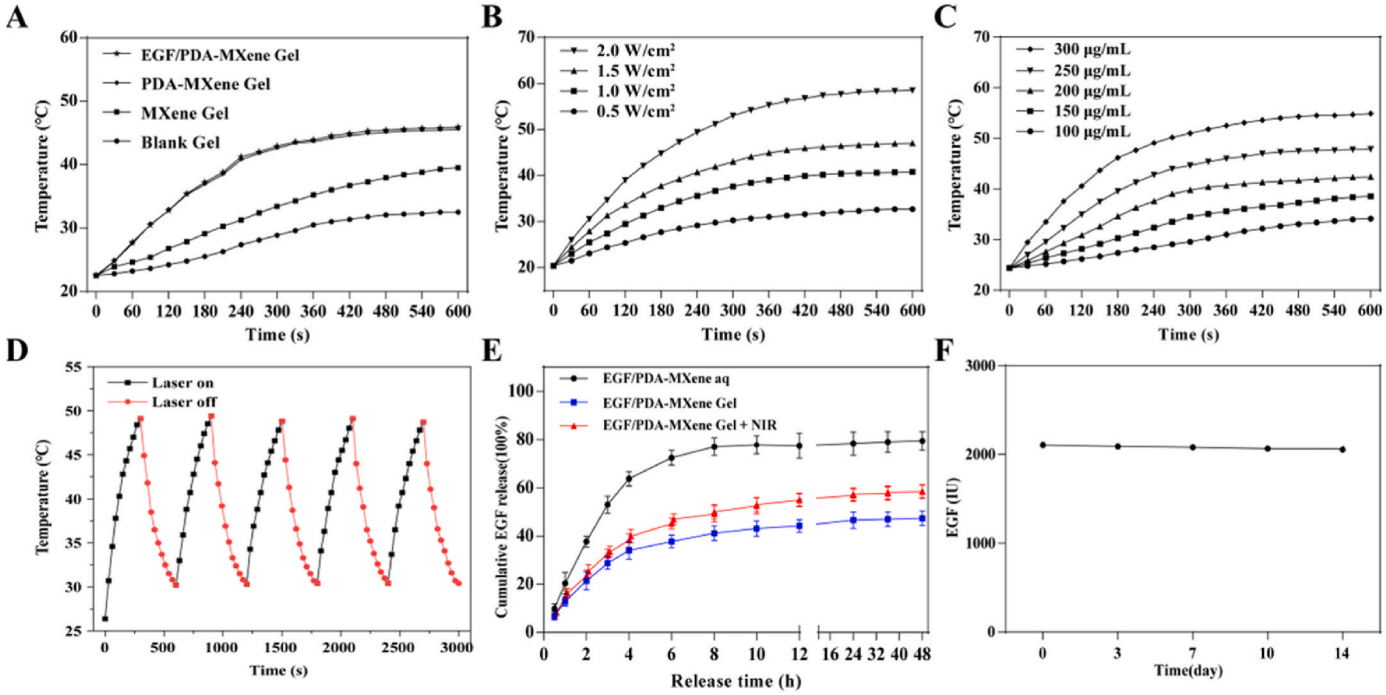

Fig. 5. Photothermal properties, in vitro drug release properties and stability of hydrogel. (A) Photothermal profiles of different hydrogels under 808 nm irradiation at 1.5 W/cm^2, (B) Photothermal profiles of EGF/PDA-MXene Gel under 808 nm irradiation at different powers, (C) Photothermal profiles of different concentrations of EGF/PDA-MXene Gel under 808 nm irradiation at 1.5 W/cm^2, (D) Photothermal profiles of EGF/PDA-MXene Gel under 808 nm irradiation at 1.5 W/cm^2 for five laser "on-off" cycles, (E) In vitro release rates of different samples at pH = 7.4, (F) EGF content change curve of EGF/PDA-MXene Gel after 14 days of standing.

3.5. Photothermal properties

The photothermal effect of different hydrogels were explored in this experiment, and the good photothermal conversion ability of MXene, accompanied by the addition of PDA, led to the further enhancement of the photothermal effects of PDA-MXene Gel and EGF/PDA-MXene Gel (Fig. 5A). The photothermal profiles of EGF/PDA-MXene Gel at different power densities showed a power density dependence, with the temperature increase becoming more pronounced as the power density increased (Fig. 5B). At a power of 0.5 W/cm^2, the Gel could not be formed rapidly within 5 min; at a power of 1 W/cm^2, the temperature increased to 40.8 °C after 10 min of irradiation, which did not meet the requirement of achieving mild thermal therapy at the wound. When the light intensity is 2 W/cm^2, the temperature is as high as 58.5 °C, affecting the physiological function of normal tissues. Therefore, 1.5 W/cm^2 was chosen for subsequent treatment. The photothermal effect of different concentrations of EGF/PDA-MXene Gel was determined at 1.5 W/cm^2. After irradiation for 5 min, the concentration could be heated up to 47.7 °C when the concentration reached 250 μg/mL, which had considerable photothermal conversion ability (Fig. 5C). In addition, the photothermal stability of the hydrogel is one of the important preparations for the evaluation of photothermal effect. After five "on-off" cycles, the temperature was stabilized at 48.9 °C after 5 min of laser irradiation, and the laser was turned off to maintain the temperature at 30 °C, which is a more comfortable temperature for human skin, and it has specific and good photothermal stability (Fig. 5D).

3.6. In vitro release performance and stability

EGF release capability of EGF/PDA-MXene solution, EGF/PDA-MXene Gel, and EGF/PDA-MXene Gel assisted by 1.5 W/cm^2 NIR were investigated respectively. The results showed that the cumulative EGF release rate of EGF/PDA-MXene solution was 79.40 % at 8 h, and the drug release rate of EGF/PDA-MXene Gel was 47.35 % at 48 h due to the hydrogen bonding between the drug and the hydrogel interior and the spatial site-blocking effect, and the release rate was significantly reduced, which indicated that the EGF/PDA-MXene Gel had a slow release effect (Fig. 5E). The brief laser-assisted action of the NIR group increased the drug release rate slightly, thus showing a small-scale "sudden release" phenomenon in the figure. After the laser was turned off, drug release continued at the original drug release, and the NIR can be regarded as a drug release switch, and the temperature increased when the laser was turned on, and the internal hydrogen bond of the hydrogel was broken, which caused the enhancement of the diffusion of the drug molecules. When the laser is switched off, the temperature drops, the hydrogen bond inside the hydrogel is restored, and the drug molecule diffusion is enhanced, causing a sudden release of the drug in a small area. This indicates that EGF/PDA-MXene Gel can achieve the slow and controlled release of drugs through the regulation of NIR, which has a broad application prospect.

EGF/PDA-MXene Gel (250 μg/mL) had a good appearance and properties after being placed at 4 °C for the 0th, 3rd, 7th, 10th, and 14th days without discoloration or sedimentation, and the pH of the gel was not affected with the increase of time (Fig. S1). The content of EGF in 1 mg of EGF/PDA-MXene nanosheets was 8332 IU as a result of the previous experiments, so the content of EGF in 250 μg/mL of EGF/PDA-MXene Gel was 2083 IU, and the content of EGF was unchanged after 14 days at 4 °C, which showed good stability (Fig. 5F).

3.7. Photothermal antimicrobial properties

S.aureus and *E.coli* were selected as the research subjects, and the antimicrobial capacity of the hydrogels was evaluated by plate coating and live/dead bacterial staining. With the administration concentration of up to 250 μg/mL, the antimicrobial effect of PDA-MXene Gel and EGF/PDA-MXene Gel on *S.aureus* was significantly enhanced compared to MXene Gel (Fig. 6A), with the antimicrobial rates as high as 93.90 ± 2.17 % and 93.95 ± 1.21 % (Fig. 6B), and the trend of the results of the staining of live/dead bacteria was roughly the same as that of live/dead bacterial staining results (Fig. 6C). Similarly, for *E. coli* (Fig. 7A), the antibacterial rate after PDA modification increased from MXene Gel 48.15 ± 6.03 % to PDA-MXene Gel 95.00 ± 3.02 % and EGF/PDA-MXene Gel 95.70 ± 2.19 %, respectively (Fig. 7B), and the red fluorescence of its live/dead bacterial staining significantly increased (Fig. 7C), indicating a stronger bactericidal effect. This may be due to the super adhesive property of PDA as a way to inhibit the growth of bacteria. The loading of the EGF did not change the antimicrobial properties of the hydrogel much and did not have an antimicrobial effect per se, but only served to keep the chances of wound infection from increasing. It should be noted that based on the excellent photothermal conversion ability of MXene and PDA, the antimicrobial effect of each experimental group was enhanced after NIR irradiation, in which the antimicrobial rates of EGF/PDA-MXene Gel against *S.aureus* and *E.coli* could be as high as 97.36 ± 2.25 % and 97.07 ± 2.36 %, respectively. The NIR group exhibited more intense red fluorescence compared with the no-NIR group, which indicated that PDA-MXene Gel and EGF/PDA-MXene Gel could better perform their antibacterial effects with the assistance of NIR light, and this result echoed the photothermal antibacterial plate counting results.

3.8. In vitro cytotoxicity and cell migration

Cell safety evaluation is one of the indispensable indexes in the safety evaluation of preparations. In the present study, mouse embryonic fibroblast L929 was selected as the target of the study, and the proliferation of the cells was detected by the CCK-8 method after 24 h and 48 h of treatment with different concentrations of drugs. The cytotoxicity of the hydrogels increased with the increase of drug concentration and incubation time, and the cell survival rate of all hydrogels was higher than 85 % at the concentration of 100 μg/mL (Fig. 8A). After 48 h of administration, MXene Gel, PDA-MXene Gel and EGF/PDA-MXene Gel showed higher cell viability compared with Blank Gel, with EGF/PDA-MXene Gel having the most significant effect, thus further demonstrating that the addition of EGF can promote the proliferation and differentiation of epidermal cells. Besides, after co-culturing the hydrogel extracts with L929 cells for 24 h and 48 h, the cells were well-grown and shuttle-shaped after treatment with the cell viability staining kit, except for the Blank Gel which showed a small amount of red fluorescence, most of the cells in the MXene Gel group, the PDA-MXene Gel group and the EGF/PDA-MXene Gel group showed green fluorescence, and only a few cells showed red fluorescence. Individual cells showed red fluorescence (Fig. 8B). This result is basically consistent with the trend of CCK-8. Overall, all groups of hydrogels showed good cytocompatibility, which lays the foundation for the subsequent preliminary pharmacodynamic validation.

The migration ability of the hydrogel to L929 cells was assessed by cell scratch repair. As time went from 0 h to 48 h, the scratch area of cells in all experimental groups decreased to varying degrees, and the MXene Gel group, PDA-MXene Gel group, and EGF/PDA-MXene Gel group showed good cell migration ability at 24 h and 48 h (Fig. 8C). Among them, the EGF/PDA-MXene Gel group had the most significant effect on promoting cell migration, with a healing rate of 87.16 ± 5.81 % after 48 h of administration (Fig. 8D), which could promote cell migration, showing a strong potential for promoting wound repair.

3.9. In vivo diabetic wound healing

In this experiment, SD male rats were selected to construct a type I diabetic wound model and comprehensively evaluate the therapeutic effect of hydrogel on chronic wounds. Blood glucose and body weight changes were monitored after STZ injection, and rats with blood glucose levels >16.6 mmol/L were selected for the construction of the diabetic

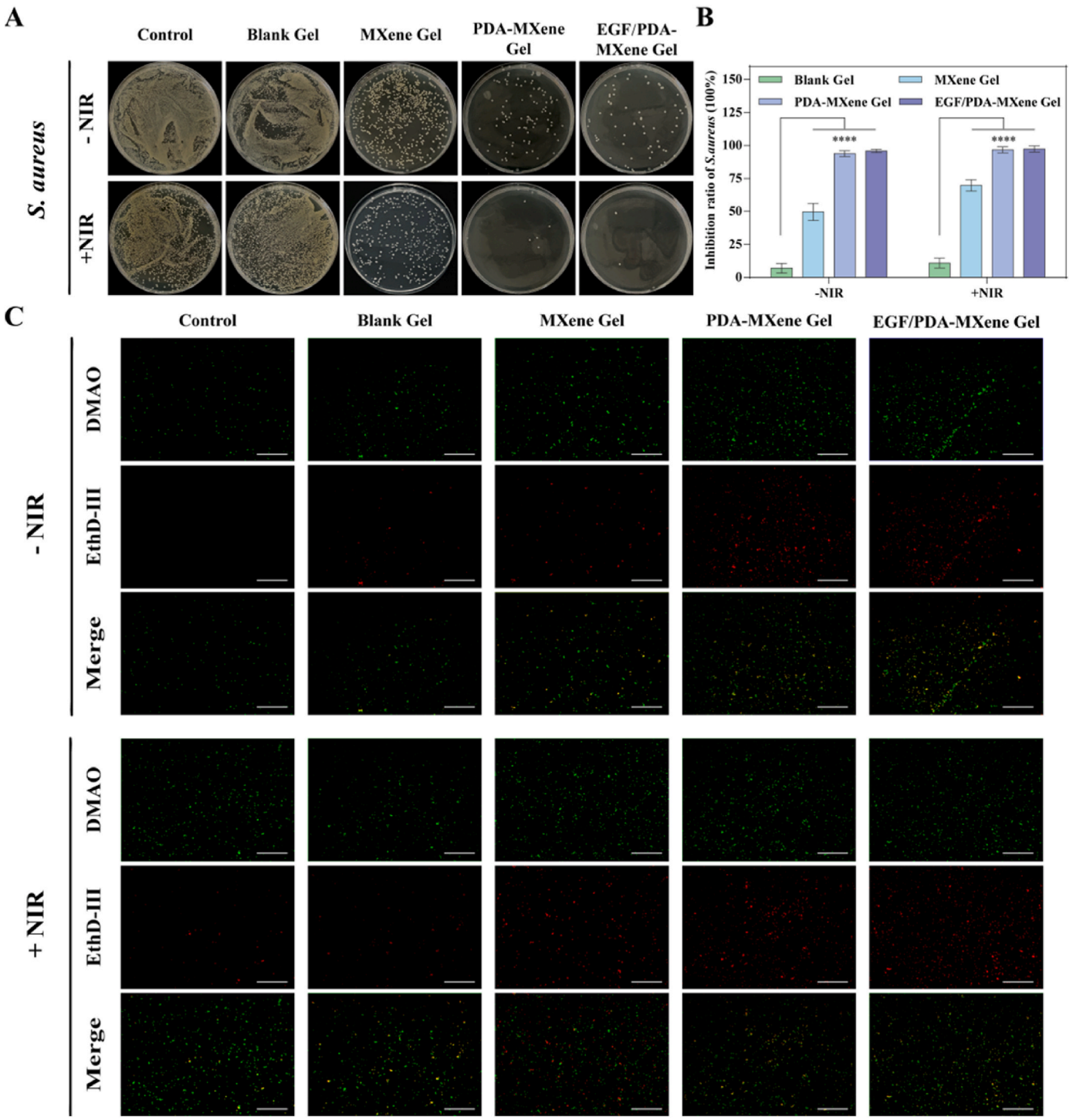

Fig. 6. Antibacterial effect of hydrogel on *S.aureus* in vitro. (A) Plate smear, (B) Inhibition rate, (C) Live/Dead bacterial staining results (scale: 100 μm).

chronic wound model (Fig. 9A). The rats showed sluggish movements, lusterless fur a significant increase in urine output, and a gradual decrease in body weight that leveled off around day 14 (Fig. 9B).

Photographs were taken on days 0, 3, 7, 10, and 14 from the time of modeling to record the wounds and fit them (Fig. 9C). After 3 days of administration, the wounds were still oozing with tissue fluid, except for the Control and Blank Gel groups, which showed the formation of thin scabs. After 7 days of treatment, the wounds of all groups had formed scabs, and the wound-healing effect of the administered group was significantly better than that of the Control group. After 14 days of treatment, the wound in the NIR group was nearly completely healed (Fig. 9D), the scabs had fallen off, and the average wound healing rate was as high as 99.14 % (Fig. 9E), accompanied by some hair growth. The above results showed that NIR irradiation could induce EGF/PDA-MXene Gel to release EGF slowly and continuously, and the local wound temperature rise and blood microcirculation increase, to accelerate the healing of chronic diabetic wounds.

3.10. Histological analysis

H&E staining and Masson staining were performed on the skin tissues on the 7th and 14th day respectively to analyze tissue regeneration

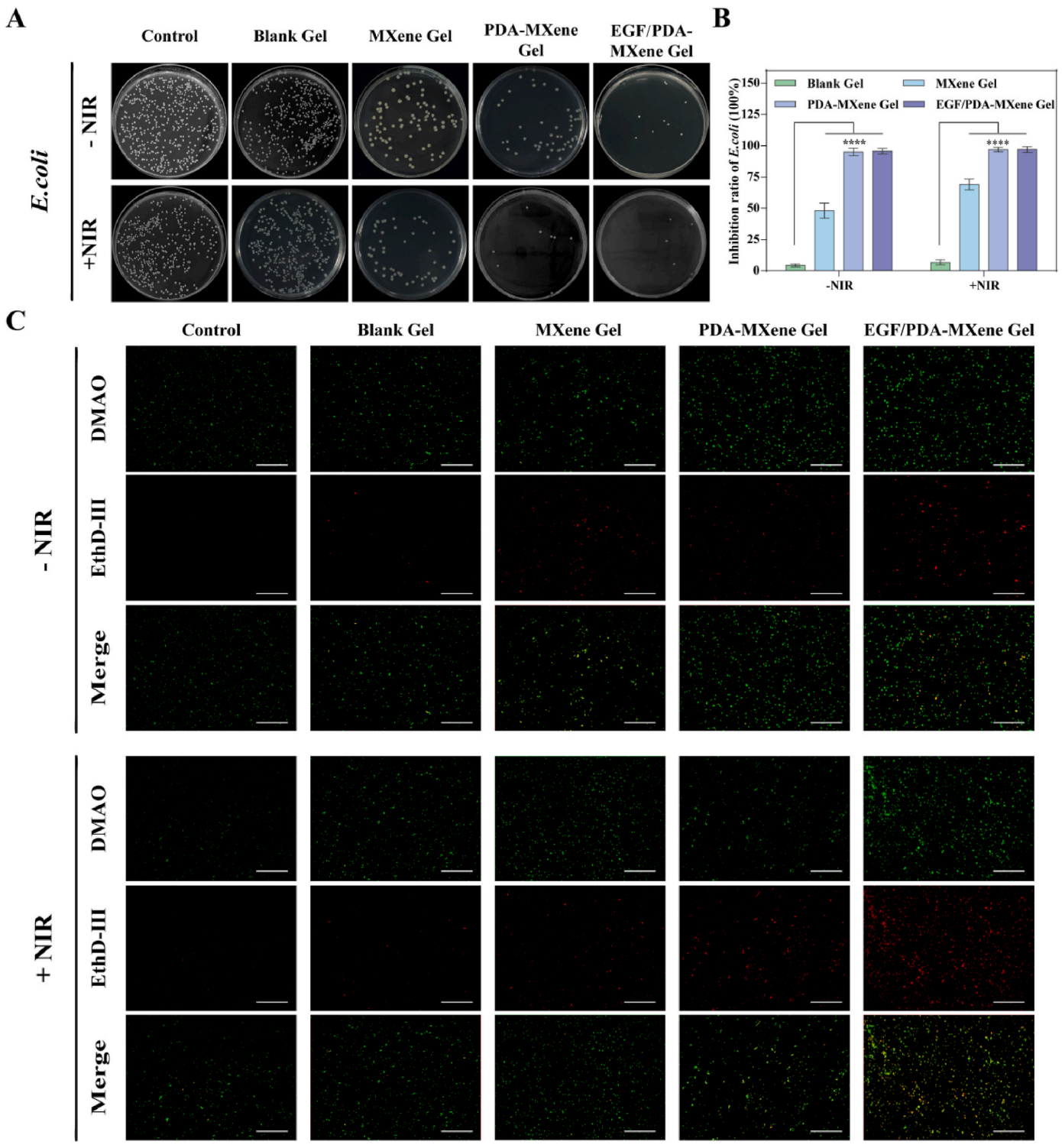

Fig. 7. Antibacterial effect of hydrogel on *E.coli* in vitro. (A) Plate smear, (B) Inhibition rate, (C) Live/Dead bacterial staining results (scale: 100 μm).

during wound healing (Fig. 10A). On day 7, more inflammatory cell infiltration (green arrows) was observed in the model group, at which time the wound was still in the inflammatory stage, whereas the EGF/PDA-MXene Gel, as well as the NIR group, had only a very small amount of inflammatory cell infiltration and some angiogenesis (red arrows). A small amount of inflammation was still present after 14 days of administration, with a significant increase in the number of neovascularization and the appearance of skin appendages such as hair follicles (blue arrows) and sebaceous glands (purple arrows) in the EGF/PDA-MXene Gel and NIR groups.

Masson staining showed that on the 7th day of administration, except for the blue collagen in the skin tissues of Blank, Control, and Blank Gel, more collagen was deposited in the other groups. After 14 days of administration, collagen fibers were evenly arranged and collagen accumulation increased in the PDA-MXene hydrogel group, the EGF/PDA-MXene hydrogel group, and the NIR group. The above results suggest that EGF/PDA-MXene Gel, assisted by NIR, accelerated the transformation of wounds from the inflammatory stage to the

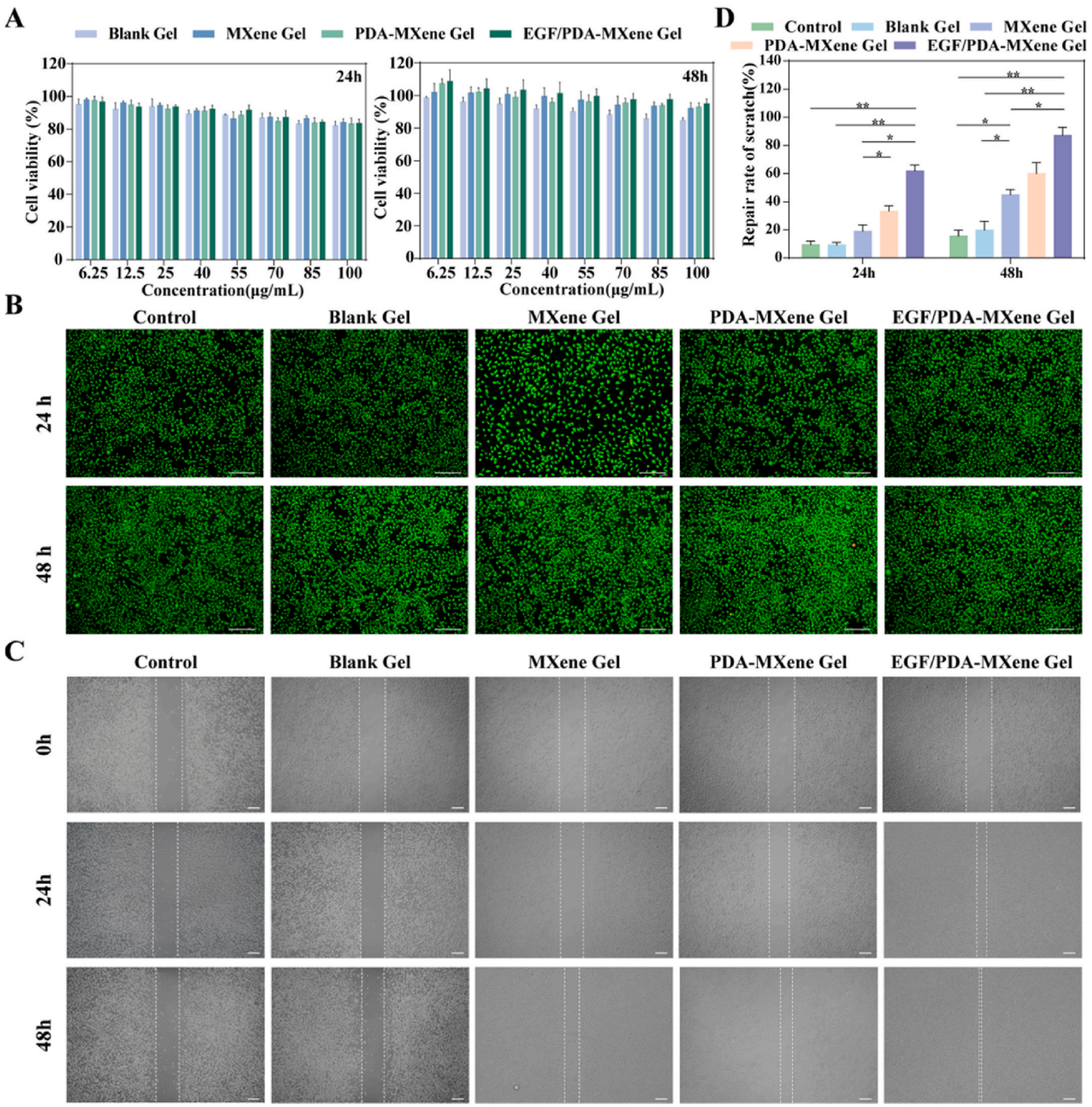

Fig. 8. Cell compatibility and cell scratching in vitro. (A) Cytotoxicity, (B) Cell live/dead staining, (C) Cell scratching, (D) Scratch area (scale: 200 μm).

proliferative stage, enhanced collagen deposition, and thus promoted diabetic chronic wound healing.

Inflammation is a necessary stage in the transition from the hemostatic to the proliferation of wound healing, and it is also a basic pathological process that occurs when the organism is subjected to external stimuli and is predominantly defensive. Two pro-inflammatory factors, IL-1β and TNF-α, were selected as the detection indexes, and immunohistochemistry was performed to evaluate the anti-inflammatory effect of hydrogel. The model group had high positive expression of IL-1β and TNF-α on day 14 of treatment, and there was a down-regulation of inflammatory cell expression in all groups with the increase of treatment time (Fig. 10B). Compared with the model group, IL-1β (Fig. 10C) and TNF-α (Fig. 10D) contents were 37.96 % and 45.09 %, respectively, EGF/PDA-MXene Gel group and NIR group had a lower positive expression, which decreased to 16.19 % and 17.97 % in NIR group. The experimental results indicated that the wound site treated with EGF/PDA-MXene Gel had less inflammation and a good anti-inflammatory effect, which could promote macrophage phenotypic transformation and thus promote diabetic chronic wound healing.

As one of the key links of wound healing, angiogenesis provides tissue with oxygen, growth factors, and immune support, thereby improving the rate of wound healing. CD31 was chosen as an index to evaluate the hydrogel angiogenesis by immunofluorescence staining. After 7 days of administration, EGF/PDA-MXene Gel and NIR groups

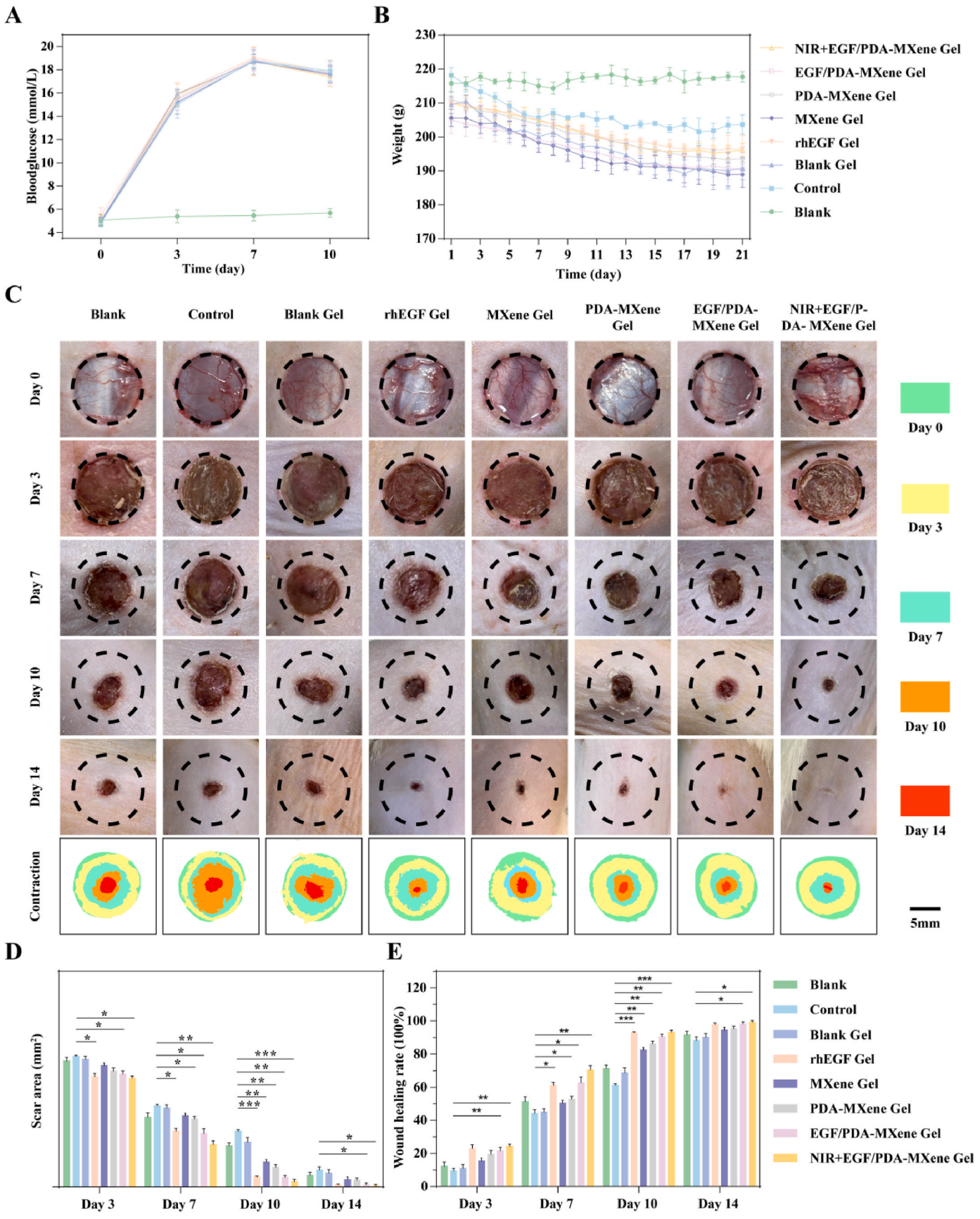

Fig. 9. In vivo wound healing experiment with hydrogels. (A) Curve of blood glucose change after STZ injection, (B) Curve of weight change, (C) Wound healing effect and wound simulation, (D) Statistical graph of wound healing area, (E) Wound healing rate.

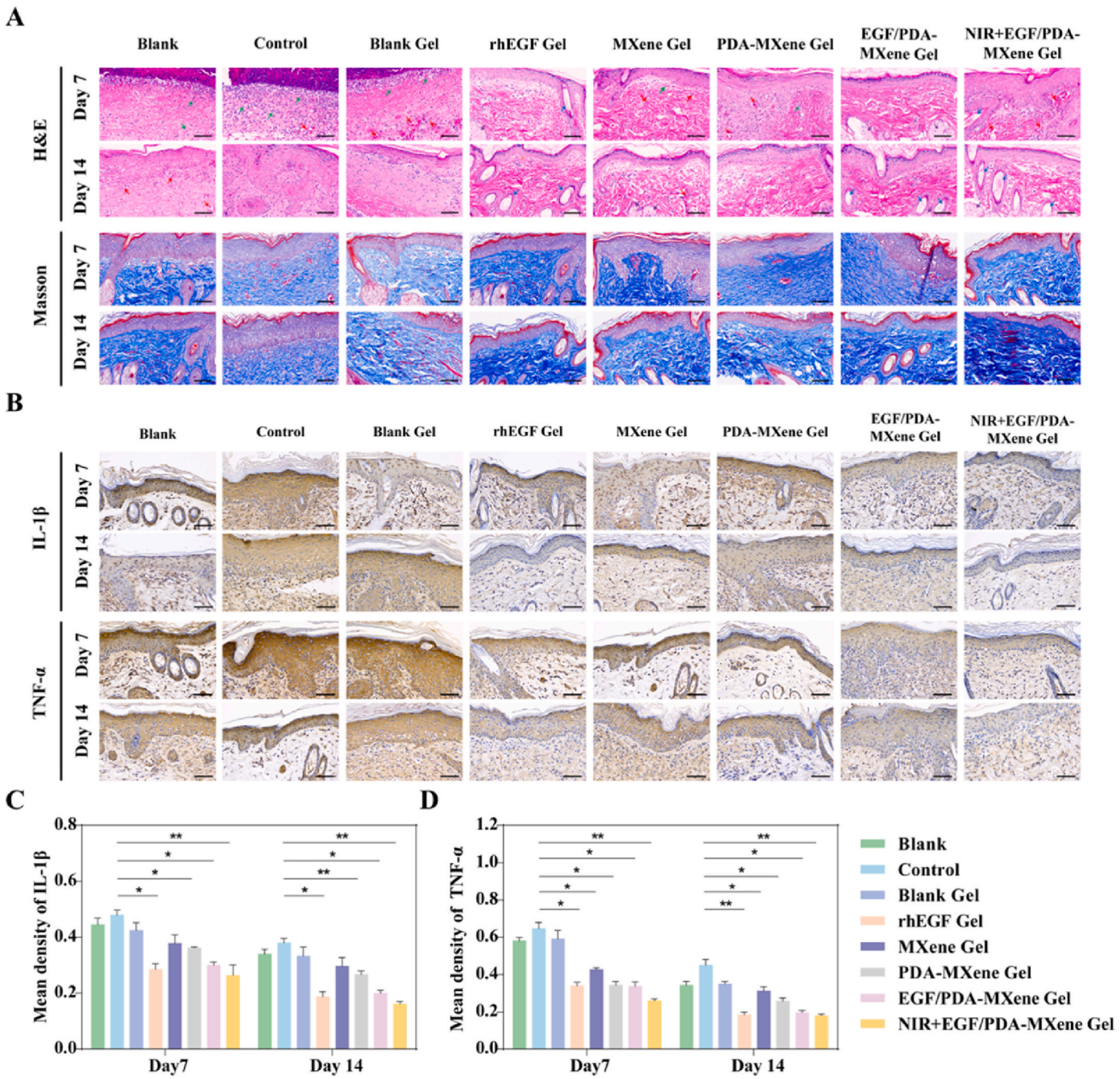

Fig. 10. Histological analysis of wounds after 7 and 14 days of treatment. (A) Histological analysis of trauma, (B) Immunohistochemical staining of skin tissue for IL-1β and TNF-α, (C) IL-1β content in skin tissue on days 7 and 14, (D) TNF-α content in skin tissue on days 7 and 14. (Scale: 200 μm).

showed strong CD31 positive expression and neovascularization, and after 14 days of administration, the number of new vessels increased and vascular fluorescent bands appeared (Fig. 11A), and the neovascularization density corresponds to 150.11 psc/mm^2 and 165.934 psc/mm^2, respectively (Fig. 11B). The above results indicated that EGF/PDA-MXene Gel could promote angiogenesis at the injury site, thus accelerating diabetic wound healing.

3.11. Biocompatibility

Good biocompatibility is one of the important conditions that the drug must have. Liver function: alanine aminotransferase (ALT), alanine aminotransferase (AST), renal function: urea nitrogen (BUN), creatinine (CREA), and blood test: red blood cell (RBC), white blood cell (WBC), platelet (PLT), and hemoglobin (HGB) in the experimental groups were examined for 14 days, and all the indexes were in normal range and there was no significant difference compared with those of the experimental groups (Fig. 12A). In addition, H&E staining of major organs did not show potential toxicity or damage (Fig. 12B). These results indicate that the hydrogel has good biocompatibility and safety during use, and can be safely and effectively applied to the treatment of diabetic chronic wounds.

4. Conclusions

In summary, this study addresses the critical issue of difficult healing in diabetic chronic wounds by constructing a NIR light-responsive nanocomposite hydrogel loaded with EGF. MXene nanosheets, a novel

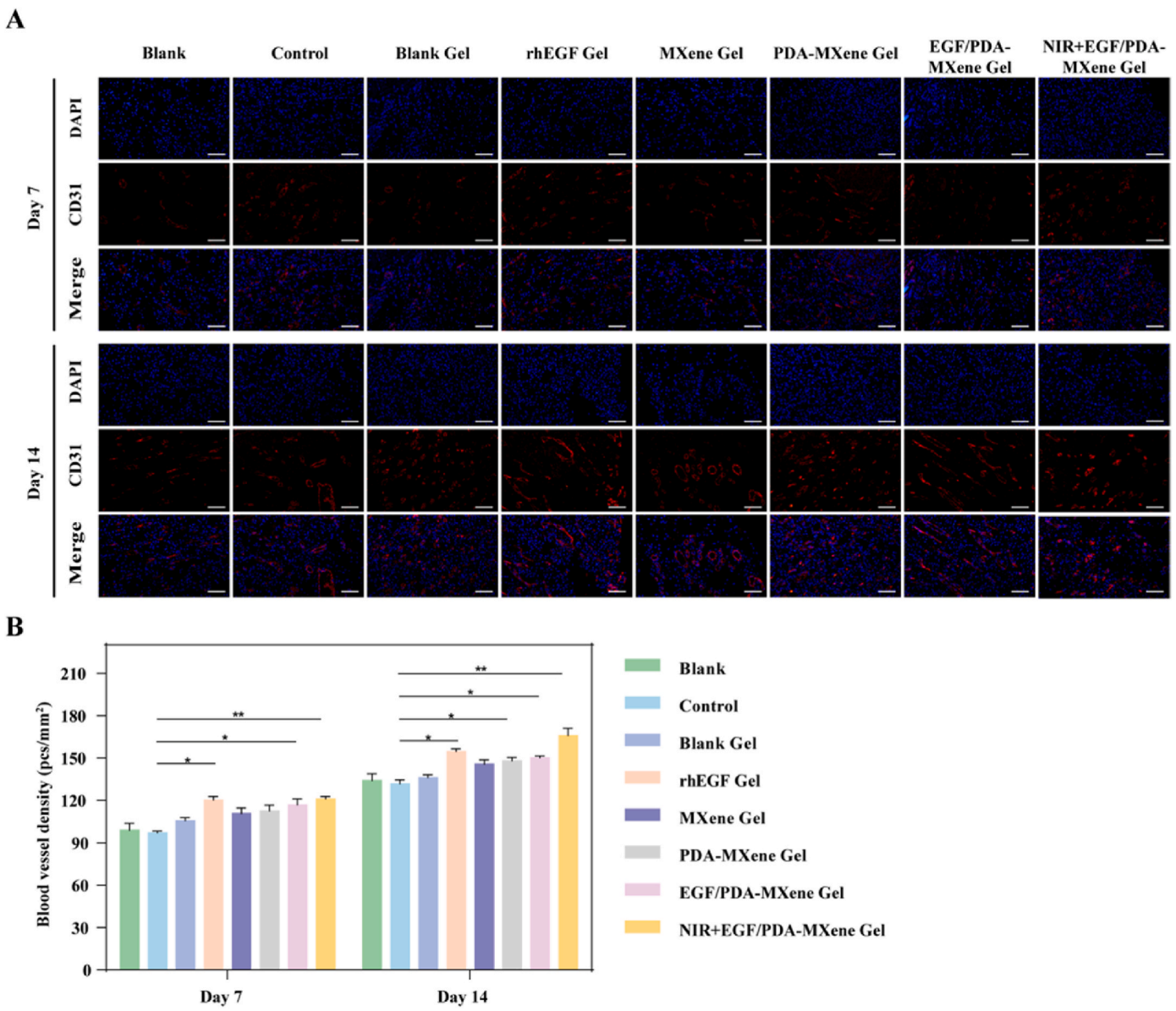

Fig. 11. Immunofluorescence analysis of angiogenic factors. (A) Immunofluorescence staining of skin tissue neovascularization on days 7 and 14, (B) CD31 content of skin tissue. (scale: 200 μm) (n = 3; $^{*}P < 0.05$, $^{**}P < 0.01$, $^{***}P < 0.001$).

2D NMs, were selected as drug carriers and modified by self-polymerization reaction under dopamine alkaline conditions to enhance the antioxidant, antimicrobial, and drug-loading capacity of MXene and to achieve EGF loading. Temperature-sensitive hydrogels with good rheological properties, skin adhesion, and stability were prepared, which can absorb tissue exudate while scavenging free radicals on the wound surface, creating a favorable environment for wound healing. In addition, the excellent photothermal properties enhanced the antimicrobial activity of EGF/PDA-MXene Gel against *S.aureus* and *E. coli*. The modulation of NIR can achieve a sustained and slow release of the drug, which can effectively inhibit the inflammatory response, accelerate the formation of granulation tissue, promote epidermal regeneration, collagen deposition, and angiogenesis, and significantly facilitate the healing of chronic diabetic wounds. Therefore, the prepared EGF/PDA-MXene Gel provides a new strategy for treating diabetic wounds and holds promise as a candidate for chronic wound healing in clinical practice.

CRediT authorship contribution statement

Li Miao: Writing – review & editing, Writing – original draft, Methodology. **Xue Lu:** Investigation, Conceptualization. **Yaoyao Wei:** Software, Resources. **Jie Zhou:** Validation, Supervision. **Yuanyuan Liu:** Visualization, Methodology. **Yang Zhang:** Validation, Methodology. **Changle Meng:** Validation, Software. **Mingyang Li:** Resources. **Hua Zhang:** Writing – review & editing, Project administration, Funding acquisition. **Wen Chen:** Writing – review & editing, Funding acquisition. **Han Zhang:** Writing – review & editing.

Ethics approval and consent to participate

This work does not involve human subjects, and it involves animal experiments. This report was approved by the Medical Ethics Committee of the First Affiliated Hospital of Shihezi University (A2023-278-01) and confirms that the authors complied with all relevant ethical regulations.

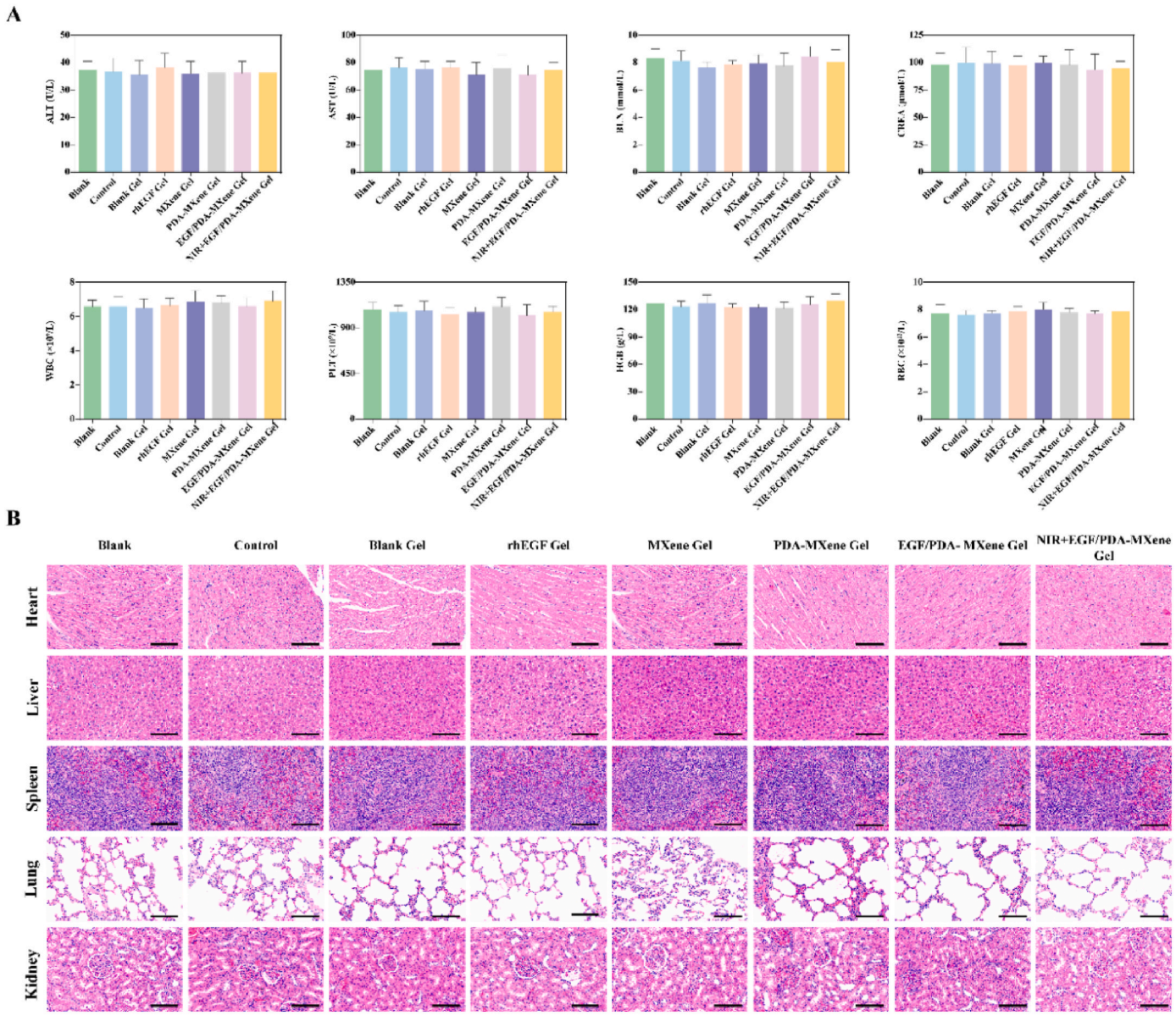

Fig. 12. Biocompatibility and safety. (A) Liver and kidney function and blood test results; (B) H&E staining of major organs (scale: 200 μm).

Declaration of competing interest

The authors declare that they have no known competing financial interests or personal relationships that could have appeared to influence the work reported in this paper.

Acknowledgments

The authors greatly acknowledge the financial support from the National Natural Science Foundation of China (Grants 82260697 and 81960648), Corps Guiding Science and Technology program projects (2022ZD052), State Key Laboratory of Natural and Biomimetic Drugs Open Subject (K202214), and Shihezi University Research Project (ZZZC202089A).

Appendix A. Supplementary data

Supplementary data to this article can be found online at https://doi.org/10.1016/j.mtbio.2025.101578.

Data availability

Data will be made available on request.

References

[1] V. Falanga, R. Rivkah Isseroff, A.M. Soulika, M. Romanelli, D. Margolis, S. Kapp, M. Granick, K. Harding, Chronic wounds, Nat. Rev. Dis. Primers 8 (1) (2022) 50.
[2] Y.-H. Lee, S.-J. Lin, Chitosan/PVA hetero-composite hydrogel containing antimicrobials, perfluorocarbon nanoemulsions, and growth factor-loaded nanoparticles as a multifunctional dressing for diabetic wound healing: synthesis, characterization, and in vitro/in vivo evaluation, Pharmaceutics 14 (2022) 537.
[3] C. He, S. Bi, R. Zhang, et al., A hyaluronic acid hydrogel as a mild photothermal antibacterial, antioxidant, and nitric oxide release platform for diabetic wound healing, J. Contr. Release 370 (2024) 543–555.
[4] Y. Kang, L. Xu, J. Dong, et al., Programmed microalgae-gel promotes chronic wound healing in diabetes, Nat. Commun. 15 (1) (2024) 1042.
[5] S. Shi, Y. Jiang, Y. Yu, et al., Piezo-augmented and photocatalytic nanozyme integrated microneedles for antibacterial and anti-inflammatory combination therapy, Adv. Funct. Mater. 33 (10) (2023) 2210850.
[6] S. Bi, C. He, Y. Zhou, et al., Versatile conductive hydrogel orchestrating neuro–immune microenvironment for rapid diabetic wound healing through peripheral nerve regeneration, Biomaterials 314 (2025) 122841.

[7] J. Jiang, X. Li, H. Li, X. Lv, Y. Xu, Y. Hu, Y. Song, J. Shao, S. Li, D. Yang, Recent progress in nanozymes for the treatment of diabetic wounds, J. Mater. Chem. B 11 (2023) 6746–6761.
[8] R. Chakraborty, P. Borah, P.P. Dutta, S. Sen, Evolving spectrum of diabetic wound: mechanistic insights and therapeutic targets, World J. Diabetes 13 (9) (2022) 696–716.
[9] M. Wu, Q. Liu, Z. Yu, M. Karvar, S. Aoki, R. Hamaguchi, C. Ma, D.P. Orgill, A. C. Panayi, Negative-pressure wound therapy induces lymphangiogenesis in murine diabetic wound healing, Plast. Reconstr. Surg. 151 (4) (2023) 779–790.
[10] Y. Wang, J.-Y. Ji, K. Guo, T. Zhang, X.-C. Zhong, Z.-M. Zhuang, Y.-F. Zhong, X.-Y. Lin, Y.-Z. Du, J. Chen, W.-Q. Tan, Gene liposome nanocomplex-loaded dermal substitute promotes diabetic chronic wound healing and angiogenesis in rat, Biomed. Pharmacother. 163 (2023) 114794.
[11] D. Pranantyo, C.K. Yeo, Y. Wu, et al., Hydrogel dressings with intrinsic antibiofilm and antioxidative dual functionalities accelerate infected diabetic wound healing, Nat. Commun. 15 (1) (2024) 954.
[12] B.M. Ertugrul, B.A. Lipsky, U. Guvenc, n. null, An assessment of intralesional epidermal growth factor for treating diabetic foot wounds, J. Am. Podiatr. Med. Assoc. 107 (1) (2017) 8750, 7315.
[13] C. Mohanty, J. Pradhan, A human epidermal growth factor-curcumin bandage bioconjugate loaded with mesenchymal stem cell for in vivo diabetic wound healing, Biomater. Adv. 111 (2020) 110751.
[14] L. Tan, Z. Hou, Y. Gao, Efficacy of combined treatment with vacuum sealing drainage and recombinant human epidermal growth factor for refractory wounds in the extremities and its effect on serum levels of IL-6, TNF-α and IL-2, Exp. Ther. Med. 15 (1) (2017) 288–294.
[15] B. Hu, M. Gao, K.O. Boakye-Yiadom, W. Ho, W. Yu, X. Xu, X.-Q. Zhang, An intrinsically bioactive hydrogel with on-demand drug release behaviors for diabetic wound healing, Bioact. Mater. 6 (12) (2021) 4592–4606.
[16] L. Miao, Y. Wei, X. Lu, M. Jiang, Y. Liu, P. Li, Y. Ren, H. Zhang, W. Chen, B. Han, W. Lu, Interaction of 2D nanomaterial with cellular barrier: membrane attachment and intracellular trafficking, Adv. Drug Deliv. Rev. 204 (2023) 115131.
[17] Z. Otgonbayar, W.-C. Oh, Comprehensive and multi-functional MXene based sensors: an updated review, FlatChem 40 (2023) 100524.
[18] M. Qin, C. Merzougui, Y.-m. Su, Y.-f. Li, W.-y. Chen, D. Huang, Recent developments in MXene and MXene/carbon composites for use in biomedical applications, N. Carbon Mater. 38 (3) (2023) 496–506.
[19] Z. Huang, X. Cui, S. Li, J. Wei, P. Li, Y. Wang, C.-S. Lee, Two-dimensional MXene-based materials for photothermal therapy, Nanophotonics 9 (8) (2020) 2233–2249.
[20] J. Meng, Z. An, Y. Liu, X. Sun, J. Li, MXene-based hydrogels towards the photothermal applications, J. Phys. Appl. Phys. 55 (37) (2022).
[21] Y. Zhong, Y. Lai, Z. Feng, S. Huang, Y. Fu, L. Huang, K.-F. Lan, A. Mo, Multifunctional MXene-doped photothermal microneedles for drug-resistant bacteria-infected wound healing, Biomater. Sci. 12 (2024) 660–673.
[22] H. An, Z. Gu, L. Zhou, S. Liu, C. Li, M. Zhang, Y. Xu, P. Zhang, Y. Wen, Janus mucosal dressing with a tough and adhesive hydrogel based on synergistic effects of gelatin, polydopamine, and nano-clay, Acta Biomater. 149 (2022) 126–138.
[23] Y. Bian, H. Wang, J. Xu, Z. Wang, X. Du, Y. Wang, Y. Du, Polydopamine–Ag composite surface guides HBMSCs adhesion and proliferation, Biomedical Materials 16 (2) (2021) 025003.
[24] P. Bai, G. Kong, W. Qiao, Y. Song, Y. Wang, J. Shi, N. Zhang, C. Liu, C. Chu, T. Xiong, Y. Zhou, C. Lu, L. Wang, N. Dong, A novel method to improve the physical property and biocompatibility of decellularized heart valve scaffold with sericin and polydopamine, Journal of Bionic Engineering 19 (2022) 1109–1123.
[25] P. Zhang, Q. Xu, J. Du, Y. Wang, Polydopamine-based nanoparticles with excellent biocompatibility for photothermally enhanced gene delivery, RSC Adv. 8 (2018) 34596–34602.
[26] R. Tang, L. Zhou, Y. Dai, Y. Wang, Y. Cai, T. Chen, Y. Yao, Polydopamine modified by pillar[5]arene in situ for targeted chemo-photothermal cancer therapy, Chem. Commun. 60 (2023) 1160–1163.
[27] C.E. Tas, E. Berksun, D. Koken, S. Unal, H. Unal, Photothermal waterborne polydopamine/polyurethanes with light-to-heat conversion properties, ACS Appl. Polym. Mater. 3 (8) 3929-3940.
[28] P. Zhang, X. Li, Q. Xu, Y. Wang, J. Ji, Polydopamine nanoparticles with different sizes for NIR-promoted gene delivery and synergistic photothermal therapy, Colloids Surf. B Biointerfaces 208 (2021) 112125.
[29] Y. Zheng, X. Chen, Q. Zhang, L. Yang, Q. Chen, Z. Chen, Y. Wang, D. Wu, Evaluation of reactive oxygen species scavenging of polydopamine with different nanostructures, Adv. Healthcare Mater. 13 (14) (2023) 2302640.
[30] H. Wang, X. Xu, X. Mei, D. Zeng, B. Ying, Z. Yu, S. Liu, R. Li, Y. Qin, 3D-printed porous PEI/TCP composite scaffolds loaded with graphdiyne oxide on the surface for bone defect repair and near-infrared light-responsive antibacterial, Mater. Des. 237 (2024) 112569.
[31] H. Wu, M. Wei, Y. Xu, Y. Li, X. Zhai, P. Su, Q. Ma, H. Zhang, PDA-based drug delivery nanosystems: a potential approach for glioma treatment, Int. J. Nanomed. 17 (2022) 3751–3775.
[32] H.-S. Jung, K.-J. Cho, Y. Seol, Y. Takagi, A. Dittmore, P.A. Roche, K.C. Neuman, Polydopamine encapsulation of fluorescent nanodiamonds for biomedical applications, Adv. Funct. Mater. 28 (33) (2018) 1801252.
[33] R. Yegappan, V. Selvaprithiviraj, A. Mohandas, R. Jayakumar, Nano polydopamine crosslinked thiol-functionalized hyaluronic acid hydrogel for angiogenic drug delivery, Colloids Surf. B Biointerfaces 177 (2019) 41–49.
[34] A. Zarepour, N. Rafati, A. Khosravi, N. Rabiee, S. Iravani, A. Zarrabi, MXene-based composites in smart wound healing and dressings, Nanoscale Adv. 6 (2024) 3513–3532.
[35] X. Bai, M. Gao, S. Syed, J. Zhuang, X. Xu, X.-Q. Zhang, Bioactive hydrogels for bone regeneration, Bioact. Mater. 3 (4) (2018) 401–417.
[36] G.M. El-Zaafarany, M.E. Soliman, S. Mansour, M. Cespi, G.F. Palmieri, L. Illum, L. Casettari, G.A.S. Awad, A tailored thermosensitive PLGA-PEG-PLGA/emulsomes composite for enhanced oxcarbazepine brain delivery via the nasal route, Pharmaceutics 10 (4) (2018) 217.
[37] Z. Zeng, Y. Li, K. Deng, D. Zou, L. Liu, B. Guo, Y. Liu, C. Shen, X. Liang, X. Xu, Thermal-cascade multifunctional therapeutic systems for remotely controlled synergistic treatment of drug-resistant bacterial infections, Adv. Funct. Mater. 34 (18) (2024) 2311315.